Cooperative Satellite-Aerial-Terrestrial Systems: A Stochastic Geometry Model

Zhe Song, Jianping An, *Senior Member, IEEE*, Gaofeng Pan, *Senior Member, IEEE*, Shuai Wang, *Senior Member, IEEE*, Haoxing Zhang, *Student Member, IEEE*, Yunfei Chen, *Senior Member, IEEE*, and Mohamed-Slim Alouini, *Fellow, IEEE*

***Abstract*— Nowadays, satellite and aerial platforms are playing an important role in realizing global seamless wireless coverage. In this paper, a cooperative satellite-aerial-terrestrial network (SATN) is considered, in which two kinds of relaying links, satellite and aerial relaying links, are used to assist a group of aerial terminals to forward their information to a remote terrestrial destination (D). Specifically, we model these aerial platforms sharing the same frequency band as a Matérn hard-core point process type-II. Also, a group of aerial jammers at D's side is modeled as a Poisson point process. To demonstrate the end-to-end (e2e) performance of the two relaying links, the statistical characteristics of the received signal-to-interference are characterized and then a closed-form expression for the outage probability (OP) over the uplink from the aerial source to the satellite/the aerial relay, the downlink from the satellite/the aerial relay to D, and the inter-aerial relay link are derived. Numerical results are presented to verify the proposed analysis models and compare the outage performance of the considered cooperative SATN with the two relay links under numerous scenarios.**

***Index Terms*— Matérn hard-core point process, outage probability, satellite-aerial-terrestrial communication, stochastic geometry.**

I. Introduction

OWING to the recent advancement of materials and manufacturing technologies in the electronics industry, satellites and aerial platforms have been deployed to serve as space and aerial relays or base stations (BS) to provide global seamless coverage. For example, thousands of low orbit satellites have already been launched into space by SpaceX to provide satellite Internet access to most of the Earth. On the other hand, in the stratosphere, high-altitude platforms, usually unmanned airships or airplanes positioned above 20 km, and low-altitude platforms, like unmanned aerial vehicles (UAVs) operating 100s to 1000s meters, have already been deployed for commercial, emergency, and military applications. However, compared with traditional ground BSs with uninterruptible power supply, satellites and aerial platforms suffer from limited power budget and hardware resources [1]–[3].

Due to the unique characteristics of satellite/aerial-terrestrial and satellite-aerial communication systems, e.g., system complexity, rapid variability, and large-scale operation space, it is crucial but challenging to optimally allocate system resources for optimal system performance, e.g., energy efficiency/power consumption, coverage, capacity/throughput, etc. For instance, recent works aim to maximize the energy efficiency/the power consumption for satellite-aerial-terrestrial networks (SATNs)/satellite-terrestrial systems [4]–[9]. Other researchers paid their attention to improving the transmission rate/the through for SATNs/satellite-terrestrial systems [10]–[12] or to achieving other optimal performance indices for SATN/satellite-terrestrial systems [13]–[17].

In practice, except from optimizing the performance of SATNs/satellite-aerial/terrestrial systems, it is also vital to thoroughly understand how such systems operate, what kinds of system factors can affect their performance, and the principles that these system factors influence the performance. Therefore, some other researchers engaged in modeling and analyzing the performance of SATNs/satellite-aerial/terrestrial systems to uncover their operation principles in numerous working scenarios.

As the most popular system architecture for the applications of communication satellites, satellite-aerial/terrestrial communications have gained considerable attention from researchers [18]–[27]. However, sometimes, the terrestrial terminals may not be able to catch the signal transmitted by the satellite over such a long-distance space-to-ground link, due to the unavailability of line-of-sight (LoS) transmissions between the satellite and the terrestrial receivers coming from the deep fading or shadowing. Moreover, increasing the transmit power at the satellite/ground-user will not be able to get out of this trouble. Intuitively, to effectively work out such

Manuscript received 17 January 2022; revised 30 May 2022; accepted 14 July 2022. Date of publication 26 July 2022; date of current version 9 January 2023. This work was supported in part by the National Natural Science Foundation of China under Grant 62171031 and Grant U1836201 and in part by the 173 Foundation under Grant XXXX-XXXX-JJ-0002. The associate editor coordinating the review of this article and approving it for publication was D. W. K. Ng. *(Corresponding author: Gaofeng Pan.)*

Zhe Song is with the School of Information and Electronics Engineering, Beijing Institute of Technology, Beijing 100081, China (e-mail: 3220195085@bit.edu.cn).

Jianping An, Gaofeng Pan, Shuai Wang, and Haoxing Zhang are with the School of Cyberspace Science and Technology, Beijing Institute of Technology, Beijing 100081, China (e-mail: an@bit.edu.cn; gfpan@bit.edu.cn; swang@bit.edu.cn; hxzhang@bit.edu.cn).

Yunfei Chen is with the School of Engineering, The University of Warwick, Coventry CV4 7AL, U.K. (e-mail: yunfei.chen@warwick.ac.uk).

Mohamed-Slim Alouini is with the Computer, Electrical and Mathematical Science and Engineering Division, King Abdullah University of Science and Technology (KAUST), Thuwal 23955-6900, Saudi Arabia (e-mail: slim.alouini@kaust.edu.sa).

Color versions of one or more figures in this article are available at https://doi.org/10.1109/TWC.2022.3192276.

Digital Object Identifier 10.1109/TWC.2022.3192276

problems, introducing relays to bridge an alternative way for the information transmissions between the satellite and terrestrial terminals will be the first but best choice.

Generally, there are two kinds of relays that have been brought to satellite communication systems: terrestrial and aerial relays. By integrating terrestrial relay, conventional satellite communication systems evolve into hybrid satellite-terrestrial relay networks (HSTRN), which have been extensively investigated. Authors of [28] derived a closed-form analytical expression of the b-th moments of the complementary cumulative distribution functions of signal-to-interference-to-noise ratio (SINR) for the satellite-to-relay link and relay-to-user link in an integrated low earth orbit (LEO) decode-and-forward (DF) millimeter-wave HSTRN. The average symbol error rate performance in a multiuser HSTRN with opportunistic scheduling was studied in [29]. In [30], the authors investigated the outage performance of a multi-relay multiuser HSTRN operating at millimeter-wave bands, while considering that the dominant fading factor of the mmWave band is rain attenuation. In [31], the bit error rate and spectral efficiency were analyzed for a multi-relay broadcast HSTRN by considering the joint impact of carrier frequency offset and phase noise. Authors of [32] derived novel and exact outage probability (OP), symbol error probability, and achievable rate expressions for a two-way HSTRN over generalized fading channels. In [33], the outage performance of non-orthogonal multiple access (NOMA)-based HSTRN was analyzed.

On the other hand, due to the flexibility of deployments, aerial relays, e.g., high and low altitude platforms including drones, air-crafts, and airships, have also been introduced into satellite-terrestrial communication scenarios to increase the probability of LoS propagation and further improve the transmission performance of satellite-terrestrial communication systems. Then, SATNs emerged as the most promising network configuration of satellite communications and are becoming a hot topic in the satellite communication area. However, the system complexity of SATNs is more complicated than that of traditional satellite-terrestrial systems, resulting in the fact that depth and extensive research is urgently required. So far, some related works have already been proposed to study the outage, capacity, symbol error, and secrecy performance of SATNs [34]–[39].

Observing these aforementioned studies, one can find that only the transmission over downlink or uplink has been investigated and the end-to-end (e2e) transmission performance has not been uncovered yet. As everyone knows, satellites normally serve as space relays for two remote ground communication partners. So, one sees that the study of the e2e transmission performance for the whole satellite communication system still keeps blank and remains to be understood.

Moreover, it is also easy to find that, till now, only very few works [4], [18]–[20], [25], [26], [34], [36] have studied the impacts of the randomness of the distributions of space/aerial/terrestrial terminals on the overall performance of these targeted systems. However, the positions of space/aerial/terrestrial terminals in SATNs exhibit strong randomness in such large-scale operation space, causing the strong randomness of the transmission distance among these terminals. Therefore, the path-loss experienced by the transmitted signal in SATNs also shows strong randomness.

Furthermore, none of these aforementioned works have studied the performance of satellite/aerial-terrestrial or satellite-aerial communication systems in presence of spatially multi-user interference (MUI)/co-channel interference, which can readily reflect the adverse characteristics of the practical large-scale three-dimensional operation space, though inter-user interference under NOMA scheme has been considered at the satellite in [23].

Inspired by such observations, this work considers a cooperative satellite-aerial-terrestrial communication (SATN) system, in which there are two relaying links to assist a group of aerial terminals to transmit their information to a remote terrestrial destination (D). Specifically, these aerial information sources are modeled by adopting the Matérn hard-core point process type-II to mimic and address the random properties of the deployment of practical aerial platforms. It is also assumed that these aerial sources access the satellite or the aerial relay while sharing the same frequency band. For example, code-division multiple access (CDMA) scheme is employed at the satellite/aerial relay due to the ability of frequency reuse, the flexibility in traffic management, and the orbit/spectrum resources. Then, the impacts of MUI have been considered over the uplink from aerial sources to the satellite/aerial relay.[1] Moreover, to address the harshness of wireless communication, a group of aerial jammers, which is modeled as a Poisson point process (PPP), are taken into consideration at D's side. The main contributions of this work are summarized as follows.

1. The statistical characteristics of the received signal-to-interference (SIR) over the aerial source-satellite/aerial relay uplink have been characterized by deriving the closed-form analytical expressions for the probability density function (PDF) and the cumulative distribution function (CDF) of SIR, while considering aerial sources accessing the satellite/the aerial relay via the same frequency channel, simultaneously.

2. The statistical characteristics of the received SIR over the satellite/aerial relay-D downlink have been characterized and the closed-form analytical expressions for the PDF and CDF of the SIR are presented, while considering hostile interfering scenarios.

3. The closed-form analytical expressions for the OP over the uplink from the aerial source to the satellite/aerial relay, the downlink from the satellite/aerial relay to D, and the inter-aerial relay link among the aerial relays are respectively derived. Then, the e2e OP for the two considered relay links is also achieved.

4. The outage performance of the considered cooperative SATN system with the two relay link under numerous scenarios are compared via numerical results, and further meaningful insights are concluded accordingly.

[1]Actually, it is very common that MUI exists in practical wireless communication systems, e.g., MUI always exists in practical CMDA systems which arises from the imperfect orthogonality existing among CDMA users or comes from the imperfect synchronization existing in time-division multiple access systems in which the users share the same frequency channel.

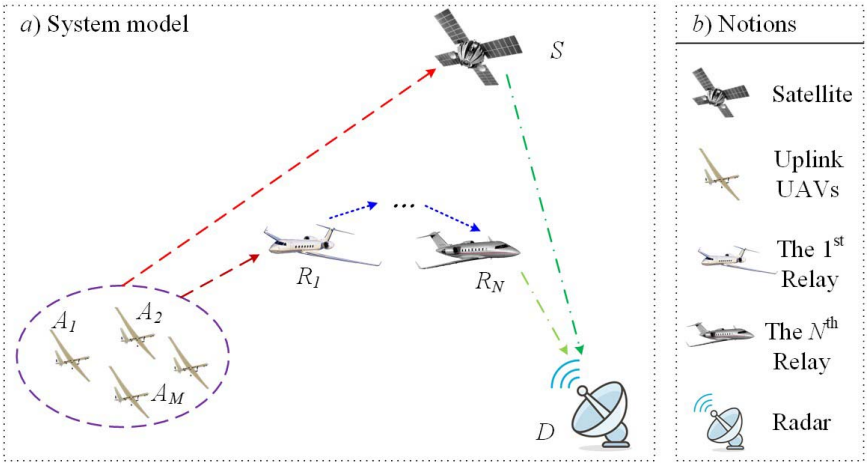

Fig. 1. Illustration of the cooperative SATN system: a) the cooperative communications with the aid of a series of aerial relays and a satellite; and b) notions.

The remainder of this work is structured as follows. In Section II, the considered system model is presented. Outage analysis of the uplink and the downlink is presented in Sections III and IV, respectively. In Section V, the OP of the inter-aerial relaying link and the e2e OP are evaluated. The proposed analytical models are verified by Monte-Carlo simulations in Section VI. Finally, the paper is concluded with some meaningful insights in Section VII.

II. System Model

In this work, we consider a cooperative SATN, which includes a satellite (S), a number of aerial relays (R_n, $n \in \mathbb{Z}^+$, $n \in [1, \cdots, N]$, $N \geq 1$), a group of aerial transmitters (A_m, $m \in \mathbb{Z}^+$, $m \in [1, \cdots, M]$, e.g., UAVs, and $M \geq 1$), and a destination (D),[2] as shown in Fig. 1. The aerial transmitters, e.g., UAVs, aim to transmit their information to a remote terrestrial destination D. However, as the distances between A_m and D are quite large, the direct links from the transmitters to the terrestrial receiver are unavailable. Therefore, satellite communications are exploited as a solution to aid the targeted remote wireless transmission.

Additionally, there is an alternative relaying link via a series of aerial relays R_n to link the aerial transmitters and D. The N aerial relays are ordered from one to N to perform cooperative transmission with $N+1$ hops.[3] Therefore, the received signals at D can be enhanced to achieve enlarged performance. We split our system into a downlink, an uplink, and inter-aerial relaying links,[4] shown in Fig. 2.

[2]In this work, we consider two types of relaying links to assist the aerial source nodes and the terrestrial destination for comparison purpose. Because both of them are possible solutions in reality to bridge the source and destination nodes which are far from each other and the two kinds of relaying links show advantages and disadvantages in transmission performance (e.g., power consumption and transmission delay) due to their transmission characteristics [21].

[3]The received signal at the other aerial relays except for the first one will not suffer MUI which exists at the first one, as the aerial relays will transmit the information of different users on orthogonal resources, e.g., time slots, to improve the transmission quality.

[4]Here, the effect of Doppler shifts at the receiver has been ignored to make the analysis more concise, as it has been well studied and is out of the main focus of our work.

A. The Uplink

For the uplink, we consider two types of channels, i.e., the channels between the aerial transmitters and aerial relays and the channels between aerial transmitters and the satellite.

1) Multi-Access Mechanism at S/R_1: As there are a group of aerial transmitters trying to deliver their information to D via the help of S/R_1, the multi-access mechanism adopted at S/R_1 is a key factor affecting the transmission performance of the uplink.

In this work, we assume that these aerial transmitters share the same frequency by using CDMA. In this case, the received signal at S/R_1 will suffer from the MUI arising from other aerial transmitters, which will be discussed in the following analysis.

2) Deployment of Aerial Transmitters: In this work, we exploit the Matérn hard-core point process (MHCPP) type-II to mimic and reflect the random deployment of practical aerial scenarios for the aerial transmitters.[5] As considered, the aerial transmitters are randomly deployed in the ball space, denoted as $\mathcal{V}$. Each candidate point has a minimum distance $D_{\min}$ to maintain aviation safety. Before presenting the detailed distributions for the candidate points, we introduce the concept of the MHCPP type-II first as follows.

We define that the locations of the candidate points have a density λ_A and each candidate point has the minimum distance $D_{\min}$. Then, we present the processes to build up a MHCPP, denoted as Φ_A, within three steps.

- In the first step, we follows the homogeneous Poisson point processes (HPPP) to initially generate the candidate points. Hence, the candidate points are randomly chosen from the space $\mathcal{V}$ with the density λ_P. If we denote the number of the candidate points as N_P, the probability mass function of the Poisson distribution with a mean $\lambda_P V$, when the number of the candidate points equals to s, can be expressed as $\Pr\{N_P = s\} = \frac{(\lambda_P V)^s}{s!} \exp(-\lambda_P V)$, where V is the volume of space $\mathcal{V}$.

[5]The MHCPP is adopted here is to accurately reflect and model the practical deployment of aerial terminals, as the aerial terminals cannot be too close to each other to promise their safety or to hold their own serving space.

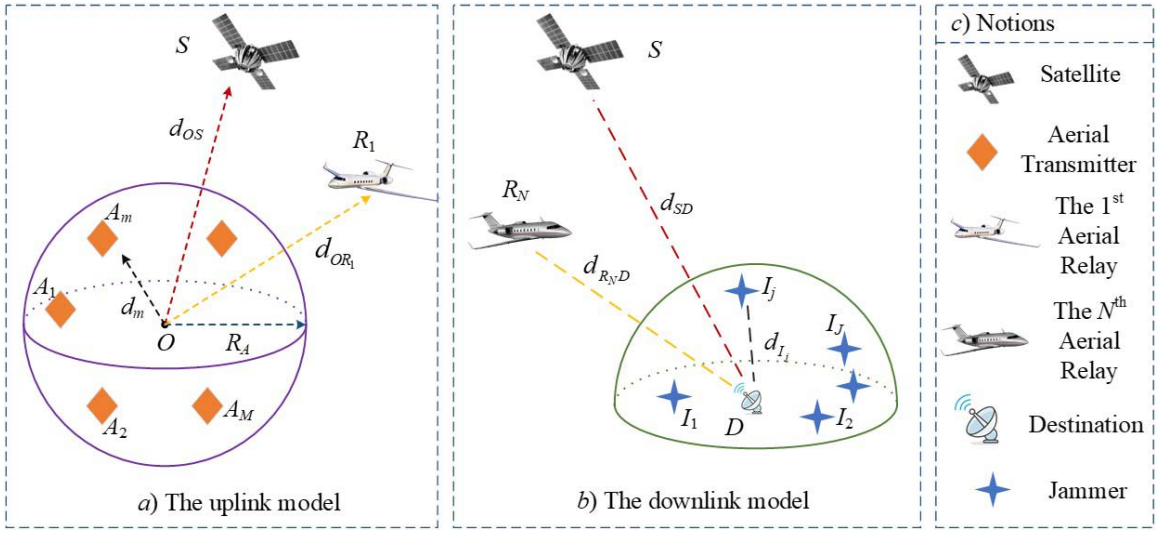

Fig. 2. Illustration of the cooperative SATN system: a) the uplink channels from the aerial sources to the satellite/the aerial relays; b) the downlink channels from the satellite/ the aerial relays to the terrestrial destination; and c) notions.

- In the second step, we generate an independent mark for each candidate point. The value of the marks is chosen based on a uniform distribution with a range from $[0, 1]$.
- In the final step, we only choose the point with the smallest mark within a small space with the distance $D_{\min}$, while the others are eliminated. More specifically for a certain point K, we choose K as the center of a small spherical repulsion space with the radius $D_{\min}$. If there are other candidate points in the spherical repulsion space, we compare the mark value from one to another. We only keep the point with the smallest mark in each spherical repulsion space. Then, we move to another candidate point to do the same processes until each spherical repulsion space has only one point. Based on this process, we have the relationship of densities, i.e., λ_A and λ_P, which is expressed as $\lambda_A = \frac{1-\exp\left(-\frac{4}{3}\pi D_{\min}^3 \lambda_P\right)}{\frac{4}{3}\pi D_{\min}^3}$.

3) Channel Fading: Though LoS propagation plays a leading role over air-to-air/space links, the path impairments in the aeronautical mobile-satellite communications include surface reflection (multi-path) effects [45]. Thus, without loss of generality and facilitating the following analysis, we assume that all uplink channels suffer independent and identically distributed (i.i.d.) Nakagami-*m* fading, which covers the statistical characteristics of LoS propagation. Hence, the expressions of the PDF and CDF are presented as

$$f_{|h_{A_mX}|^2}(x) = \left(\frac{m_n}{\Omega}\right)^{m_n} \frac{x^{m_n-1}}{(m_n-1)!} \exp\left(-\frac{m_n}{\Omega}x\right) \quad (1)$$

and

$$F_{|h_{A_mX}|^2}(x) = 1 - \sum_{i=0}^{m_n-1} \left(\frac{m_n}{\Omega}\right)^{m_n-i-1} \frac{x^{m_n-i-1}}{(m_n-i-1)!} \times \exp\left(-\frac{m_n}{\Omega}x\right), \quad (2)$$

respectively, where $X \in \{S, R_1\}$ to present the satellite and the first aerial relay, respectively, $|h_{A_mX}|^2$ is the channel gain of the channel from the aerial transmitter A_m to the relay or the satellite, X, and m_n and Ω is the parameters of Nakagami-*m* fading channels.

4) Signal Model: We consider a practical satellite-aerial-terrestrial scenario where the aerial transmitters suffer the interference from each other. Hence, the SINR for an aerial transmitter A_m to $X \in \{S, R_1\}$ can be expressed as

$$\gamma_{A_mX} = \frac{P_{A_m}|h_{A_mX}|^2 d_{A_mX}^{-\alpha_X}}{\sigma^2 + \sum\limits_{k=1\&k\neq m}^{M} P_{A_k}|h_{A_kX}|^2 d_{A_kX}^{-\alpha_X}} \approx \frac{P_{A_m}|h_{A_mX}|^2 d_{A_mX}^{-\alpha_X}}{\sum\limits_{k=1\&k\neq m}^{M} P_{A_k}|h_{A_kX}|^2 d_{A_kX}^{-\alpha_X}}, \quad (3)$$

where P_{A_m} is the transmit power at A_m, d_{A_mX} is the distance from A_m to the relay or the satellite X, α_X is the path loss exponent for the channel to the relay or the satellite, and σ^2 is the strength of additive white Gaussian noise (AWGN).

B. The Downlink

In this work, it is assumed that we exploit the decode-and-forward (DF) relay scheme to process and transmit the signals. Over the downlink, the signals from the aerial transmitters have been decoded and re-transmitted by the satellite or the aerial relays. At the terrestrial destination, we consider that there are a group of near-ground aerial jammers, denoted as I_j with $j \in \mathbb{Z}^+$ and $j \in [1, \cdots, J]$ $(J \geq 1)$, interfering the signals transmitted from the satellite or the aerial relay.

1) Deployment of Aerial Jammers: We consider that these aerial jammers follow a PPP,[6] which are uniformly distributed

[6]Here, for the downlink, the interference may not only come from the hostile neighboring terminals distributed in the considered space but also be the ones which are non-hostile and do not locate in the considered interfering space. For the later ones, the interferer may be far away from the receiver, but we can cast it into the considered hemisphere region by varying the transmission power. In this way, the interferer may be coincide in the hemisphere. Thus, the aerial jammers are modeled with normal PPP without restriction on the inter-node distance to reflect the worst case possibly existing in the practice.

in a hemisphere, $\mathcal{V}_h$, whose bottom is on the ground with the radius R_I and the original, D. The number of the aerial jammers is Poisson distributed with density λ_J, i.e., $\Pr\{N=k\} = \left(\mu_{\mathcal{V}_h}^k/k!\right)\exp\left(-\mu_{\mathcal{V}_h}\right)$, where $\mu_{\mathcal{V}_h} = \frac{2\pi {R_I}^3}{3}\lambda_J$ is the mean measure.

Define the distance from a jammer I_j to the center of the hemisphere, D, as d_{I_j}. The PDF of d_{I_j} is expressed as

$$f_{d_{I_j}}(x) = \begin{cases} 0, & x < 0; \\ \dfrac{3x^2}{R_I^3}, & 0 \leqslant x \leqslant R_I; \\ 0, & x > R_I. \end{cases} \tag{4}$$

2) Channel Fading: For the $S-D$ and $R_N - D$ links, we consider the Shadowed-Rician model, which has been widely utilized by the researches in satellite/aerial-terrestrial communication area. We denote the channel gains between S and D, and R_N and D as $|h_{iD}|^2$ ($i \in \{S, R_N\}$), thus the PDF of $|h_{iD}|^2$ is expressed as [41]

$$f_{|h_{iD}|^2}(x) = \chi \exp(-\beta x)\, {}_1F_1(m_n; 1; \delta x), \tag{5}$$

where $\chi = \left(\frac{2bm_n}{2bm_n+\Theta}\right)^{m_n} \Big/ (2b)$, $\beta = \frac{1}{2b}$, $\delta = \frac{\Theta}{2b(2bm_n+\Theta)}$, Θ and $2b$ are the average power for the line of sight component and the multi-path component, respectively, m_n is the fading parameters based on the Nakagami-m fading channels, and ${}_1F_1(\cdot;\cdot;\cdot)$ is the confluent hypergeometric function of the first kind.[7]

Moreover, for the jamming links between the aerial jammers and D, without loss of generality, it is also assumed that all jamming channels suffer i.i.d. Nakagami-*m* fading to facilitate the following analysis since LoS propagation always plays a key role in aerial-to-ground transmission scenarios.

3) Signal Model: For the $S-D$ and $R_N - D$ links, the SINR of $|h_{iD}|^2$ ($i \in \{S, R_N\}$) is

$$\gamma_{iD} = \frac{P_S |h_{iD}|^2 d_{iD}^{-\alpha_S}}{\sum_{j=1}^{J} P_j |h_{jD}|^2 d_{I_j}^{-\alpha_S} + \sigma^2} \approx \frac{P_S |h_{iD}|^2 d_{iD}^{-\alpha_S}}{\sum_{j=1}^{J} P_j |h_{jD}|^2 d_{I_j}^{-\alpha_S}}, \tag{6}$$

where P_i is the transmit power at i, P_j is the transmit power at the jth aerial jammer, d_{iD} is the distance between i and D, and α_S is the path-loss exponent.

C. Inter-Aerial Relaying Links

1) Channel Fading: In this work, it is assumed that all inter-aerial relaying links suffer Nakagami-*m* fading channels, which covers typical LoS propagation scenarios. Hence, the expressions of PDF and the CDF of the channel power gain between the nth ($n = 1, \cdots, N-1$) and the $(n+1)$th aerial relays, $\left|h_{R_n R_{n+1}}\right|^2$, are presented as

$$f_{\left|h_{R_n R_{n+1}}\right|^2}(x) = \left(\tfrac{m_n}{\Omega}\right)^{m_n} \tfrac{x^{m_n-1}}{(m_n-1)!} \exp\left(-\tfrac{m_n}{\Omega}x\right). \tag{7}$$

[7]The altitude dependent shadowing can be analysed by converting the fading parameters. Here, the effect of elevation angle on the Shadowed-Rician model has been ignored for simplification purpose, which have been well studied and is out of the main focus of our work.

2) Signal Model: Next, we present the SNR over the link between the nth ($n = 1, \cdots, N-1$) and the $(n+1)$th aerial relays as $\gamma_{R_n R_{n+1}} = \frac{P_{R_n}\left|h_{R_n R_{n+1}}\right|^2}{d_{R_n R_{n+1}}^{\alpha_{R_N}} \sigma^2}$, where P_{R_n} is the transmit power at the nth aerial relay, $d_{R_n R_{n+1}}$ is the distance between the nth and the $(n+1)$th aerial relays, and α_{R_n} is the path-loss exponent.

III. Outage Analysis of the Uplink

For simplification, assume that all the aerial transmitters except the target transmitter share the same transmit power with $P_{A_k} = P_{A_u}$ and denote $m_i = m_n - i - 1$.

Lemma 1: The OP for the received signal at X ($X \in \{S, R_1\}$), which is transmitted by the mth aerial transmitter, can be derived as

$$P_{out}^{A_m X} = 1 - \sum_{i=0}^{m_n-1} \frac{(-1)^{m_i}}{(m_i)!} \mathbb{E}_{d_{A_m X}} \left\{ s^{m_i} \frac{\mathrm{d}^{m_i} \mathbb{E}_I\{\exp(sI)\}}{\mathrm{d}s^{m_i}} \right\}, \tag{8}$$

where $I = \sum_{k=1 \& k \neq m}^{M} |h_{A_k X}|^2 d_{A_k X}^{-\alpha_X}$ *and* $s = -\frac{m_n d_{A_m X}^{\alpha_X} \gamma_{out} P_{A_u}}{P_{A_m} \Omega}$.

Proof: Please refer to Appendix A. ∎

To obtain a closed-form expression for (8), $\frac{\mathrm{d}^{m_i}\mathbb{E}_I\{\exp(sI)\}}{\mathrm{d}s^{m_i}}$ should be calculated. Thus, we need to first derive $\mathbb{E}_I\{\exp(sI)\}$.

Lemma 2: $\mathbb{E}_I\{\exp(sI)\}$ *can be expressed as*

$$\mathbb{E}_I\{\exp(sI)\} = \exp[\lambda_A V_1 (D_2 - 1)], \tag{9}$$

where $V_1 = \frac{4\pi}{3}(R_A^3 - D_{\min}^3)$ *and* $D_2 = \mathbb{E}_{d_{A_k X}}\left\{ \left(\frac{\frac{m_n}{\Omega s} d_{A_k X}^{-\alpha_X}}{\frac{m_n}{\Omega s} d_{A_k X}^{-\alpha_X} - 1} \right)^{m_n} \right\}$.

Proof: Please refer to Appendix B ∎

Lemma 3: The OP is

$$P_{out}^{A_m X} = 1 - \sum_{i=0}^{m_n-1} \frac{1}{(m_i)!} \mathbb{E}_{d_{A_m X}} \left\{ \left(\frac{m_n d_{A_m X}^{\alpha_X} \gamma_{out} P_{A_u}}{P_{A_m} \Omega} \right)^{m_i} \times \exp[\lambda_A V_1 (D_2 - 1)] \left[1 + \mathbb{1}\{m_i > 0\} \sum_{k=1}^{m_i} B_{m_i,k} \times \left(\lambda_A V_1 D_2^{(1)}, \ldots, \lambda_A V_1 D_2^{(m_i - k + 1)} \right) \right] \right\}, \tag{10}$$

where $\mathbb{1}\{\cdot\}$ *is the indicator function and* $D_2^{(k)}$ ($k = 0, 1, \ldots, m_i$) *is*

$$D_2^{(k)} = \frac{(m_n + k - 1)!}{(m_n - 1)!} \mathbb{E}_{d_{A_k X}} \left\{ \left(\frac{\Omega}{m_n d_{A_k X}^{\alpha_X}} \right)^k \times \left(\frac{d_{A_k X}^{\alpha_X}}{d_{A_k X}^{\alpha_X} + \frac{d_{A_m X}^{\alpha_X} \gamma_{out} P_{A_u}}{P_{A_m}}} \right)^{m_n + k} \right\}. \tag{11}$$

Proof: Please refer to Appendix C. ∎

A. Uplink With the Satellite

When the aerial transmitters communicate with the satellite, we assume that all the aerial transmitters have the same transmission distance d_{OS}.[8] By substituting $d_{A_mX} = d_{OS}$ and $d_{A_kX} = d_{OS}$ into (10), we can get the OP of the uplink from the aerial transmitter cluster to the satellite as

$$P_{out}^{OS} = 1 - \sum_{i=0}^{m_n-1} \frac{1}{(m_i)!}\left(\frac{m_n d_{OS}^{\alpha_S}\gamma_{out}P_{A_u}}{P_{A_m}\Omega}\right)^{m_i} \times \exp\left[\lambda_A V_1(D_2-1)\right]\left[1+\mathbb{1}\{m_i>0\}\sum_{k=1}^{m_i} B_{m_i,k} \times \left(\lambda_A V_1 D_2^{(1)},\ldots,\lambda_A V_1 D_2^{(m_i-k+1)}\right)\right], \quad (12)$$

where $D_2^{(k)}$ $(k = 0,1,\ldots,m_i)$ is $D_2^{(k)} = \frac{(m_n+k-1)!}{(m_n-1)!}\left(\frac{\Omega}{m_n d_{OS}^{\alpha_S}}\right)^k \left(\frac{1}{1+\frac{\gamma_{out}P_{A_u}}{P_{A_m}}}\right)^{m_n+k}$.

B. Uplink With the Aerial Relay

In this case, we suppose the transmitter is located in the center of the aerial transmitter cluster and the distance from the cluster center to the aerial relay is a constant, namely, $d_{A_mR_1} = d_{OR_1}$.

To get $D_2^{(k)}$, we should derive the PDF of $d_{A_kR_1}$.

Lemma 4: The PDF of $d_{A_kR_1}^2$ is

$$f_{d_{A_kR_1}^2}(x) = \frac{\pi[R_A^2 - \tau(x)^2]}{2V_1 d_{OR_1}}, \quad (13)$$

where $\tau(x) = \max\{D_{\min}, |\sqrt{x} - d_{OR_1}|\}$ and $d_{\max}^d = (d_{OR_1} - R_A)^2 \le x \le (d_{OR_1}+R_A)^2 = d_{\max}^u$.

Proof: Please refer to Appendix D. ∎

Then, by denoting $\Lambda = \frac{d_{OR_1}^{\alpha_{R_1}}\gamma_{out}P_{A_u}}{P_{A_m}}$, $D_2^{(k)}$ in (45) can be achieved as (14), shown at the bottom of the next page.

When $\tau(x) = D_{\min}$ which means $D_{\min} > |\sqrt{x} - d_{OR_1}|$, we can get $d_{\min}^d = (d_{OR_1} - D_{\min})^2 < x < (d_{OR_1} + D_{\min})^2 = d_{\min}^u$ and $R_A^2 - \tau(x)^2 = R_A^2 - D_{\min}^2$.

When $\tau(x) = |\sqrt{x} - d_{OR_1}|$ which indicates $|\sqrt{x} - d_{OR_1}| > D_{\min}$, thus $(d_{OR_1} - R_A)^2 < x < (d_{OR_1} - D_{\min})^2$, $(d_{OR_1} + D_{\min})^2 < x < (d_{OR_1} + R_A)^2$, and $R_A^2 - \tau(x)^2 = R_A^2 - d_{OR_1}^2 - x + 2d_{OR_1}\sqrt{x}$.

By using [42, Eq. (3.194.1)], $D_2^{(k)}$ can be obtained as (15), shown at the bottom of the next page, where $\mathcal{F}(a,b,c,k) = \frac{2}{(m_n+a)\alpha_{R_1}}\left[b^{\frac{(m_n+a)\alpha_{R_1}}{2}} {}_2F_1 m_n+k, m_n+am_n+a+1-\frac{b^{\frac{\alpha_{R_1}}{2}}}{\Lambda} - c^{\frac{(m_n+a)\alpha_{R_1}}{2}} {}_2 1 m_n+k, m_n+am_n+a+1-\frac{c^{\frac{\alpha_{R_1}}{2}}}{\Lambda}\right]$ and the detailed derivation of (15) is given in Appendix E.

Substituting (15) and $d_{A_mX} = d_{OR_1}$ into (10), we can get the OP over the uplink from the aerial transmitter to the first aerial relay as

$$P_{out}^{OR_1} = 1 - \sum_{i=0}^{m_n-1} \frac{1}{(m_i)!}\left(\frac{m_n d_{OR_1}^{\alpha_X}\gamma_{out}P_{A_u}}{P_{A_m}\Omega}\right)^{m_i} \times \exp\left[\lambda_A V_1(D_2-1)\right]\left[1+\mathbb{1}\{m_i>0\}\sum_{k=1}^{m_i} B_{m_i,k} \times \left(\lambda_A V_1 D_2^{(1)},\ldots,\lambda_A V_1 D_2^{(m_i-k+1)}\right)\right]. \quad (16)$$

Interestingly, comparing (12) and (16), we can find that the closed-form analytical expression for the OP over the uplink from the aerial transmitter to the satellite is similar to that for the OP over the uplink from the aerial transmitter to the aerial relay. Thus, in Section VI, we will study the outage performance of the uplink by merging these two cases into one for simplicity.

C. Asymptotic Outage Performance of the Uplink

In this part, we will present the asymptotic analysis of the outage performance of the uplink of the considered system. In the following, we derive the approximate expressions assuming $\lambda = \frac{P_{A_mX}}{N_0} \to \infty$.

Adopting the series representations of the exponential function, $\exp\left(-\frac{m_n x}{\Omega}\right) = \sum_{n=0}^{\infty}\frac{\left(-\frac{m_n x}{\Omega}\right)^n}{n!}$, and keeping the first two terms while ignoring the higher order term, the asymptotic CDF of $\lambda|h_{A_mX}|^2$ can be obtained as

$$F_{\lambda|h_{A_mX}|^2}^{\infty}(x) = 1 - \sum_{i=0}^{m_n-1}\left(\frac{m_n}{\Omega}\right)^{m_n-i-1}\frac{x^{m_n-i-1}}{(m_n-i-1)!} \times \left(1-\frac{m_n x}{\Omega\lambda}\right). \quad (17)$$

Lemma 5: The asymptotic outage probability can be presented as

$$P_{out}^{\infty} = 1 - \sum_{i=0}^{m_n-1}\frac{(-1)^{m_i}}{(m_i)!}\left\{\mathbb{E}_{d_{A_mX}}\{s^{m_i}\}\mathbb{E}_I\{I^{m_i}\} - \mathbb{E}_{d_{A_mX}}\{s^{m_i+1}\}\mathbb{E}_I\{I^{m_i+1}\}\right\}, \quad (18)$$

where

$$\mathbb{E}_I\{I\} = \sum_{M=0}^{\infty}\frac{(\lambda_A V_1)^M}{(M-1)!}\exp(-\lambda_A V_1) \times \left\{1 - \sum_{i=0}^{m_n-1}\left(\frac{m_n}{\Omega}\right)^{m_n-i-1}\frac{x^{m_n-i}}{(m_n-i-1)!} \times \exp\left(-\frac{m_n}{\Omega}x\right)\right\}\mathbb{E}_{d_{A_kX}}\left\{d_{A_kX}^{-\alpha_X}\right\} \quad (19)$$

and

$$\mathbb{E}_{d_{A_mX}}\{s\} = \mathbb{E}_{d_{A_mX}}\left\{-\frac{m_n d_{A_mX}^{\alpha_X}\gamma_{out}P_{A_u}}{P_{A_m}\Omega}\right\}. \quad (20)$$

Proof: Please refer to Appendix F. ∎

When the aerial transmitters communicate with the satellite, $\mathbb{E}_I\{I\}$ can be further derived as

$$\mathbb{E}_I\{I\} = \sum_{M=0}^{\infty}\frac{(\lambda_A V_1)^M}{(M-1)!}\exp(-\lambda_A V_1)$$

[8]This assumption is reasonable since the distance to the satellite (normally on the order of hundreds/thousands of km) is quite larger than that to each other (normally on the order of km to tens of km).

$$\times \left\{ 1 - \sum_{i=0}^{m_n-1} \left(\frac{m_n}{\Omega}\right)^{m_n-i-1} \frac{x^{m_n-i}}{(m_n-i-1)!} \times \exp\left(-\frac{m_n}{\Omega}x\right) \right\} d_{A_kX}^{-\alpha_X}. \quad (21)$$

Thus, P_{out}^{∞} can be rewritten as

$$P_{out}^{\infty} = 1 - \sum_{i=0}^{m_n-1} \frac{(-1)^{m_i}}{(m_i)!} \left\{ s^{m_i} \{\mathbb{E}_I\{I\}\}^{m_i} - s^{m_i+1} \{\mathbb{E}_I\{I\}\}^{m_i+1} \right\}, \quad (22)$$

When the aerial transmitters communicate with the aerial relay, we can obtain $\mathbb{E}_{d_{A_kX}}\left\{d_{A_kX}^{-\alpha_X}\right\}$ as (23), shown at the bottom of the next page.

Thus, we can obtain the asymptotic OP over the uplink from the aerial transmitter to the satellite by substituting (23) into (18).

IV. Outage Analysis of the Downlink

Similar to Section III, the OP of the downlink depicted in Fig. 2(b) can be given as

$$P_{out}^{iD} = \Pr\{\gamma_{iD} \le \gamma_{out}\} \approx \Pr\left\{ \frac{P_i |h_{iD}|^2 d_{iD}^{-\alpha_S}}{\sum_{j=1}^{J} P_j |h_{jD}|^2 d_{I_j}^{-\alpha_S}} \le \gamma_{out} \right\}, \quad i \in \{S, R_N\}. \quad (24)$$

Moreover, as the focus of this section is to investigate the impacts of these spatial distribution aerial jammers on the outage performance of the downlink, here we also assume that the distance between the satellite/the last aerial relay and D is fixed for the feasibility of the analysis. Namely, d_{iD} ($i \in \{S, R_N\}$) is with a given value. Thus, we can rewrite the previous equation as

$$P_{out}^{iD} = \Pr\left\{ \frac{Z}{Y} \le \frac{d_{iD}^{\alpha_S}}{P_i} \gamma_{out} \right\}, \quad (25)$$

where $i \in \{S, R_N\}$, $Z = |h_{iD}|^2$, and $Y = \sum_{j=1}^{J} P_j |h_{jD}|^2 d_{I_j}^{-\alpha_S}$.

Recalling (5) and using the Kummer's transform of the hypergeometric function, we easily rewrite the PDF of $|h_{iD}|^2$ as $f_{|h_{iD}|^2}(x) = \sum_{k=0}^{m_n-1} \Psi(k) x^k \exp(-(\beta-\delta)x)$, where $\Psi(k) = \delta^k \frac{(-1)^k}{(k!)^2} \chi (1-m_n)_k$ and $(\cdot)_n$ is the Pochhammer symbol. Then, the CDF of $|h_{iD}|^2$ can be presented as

$$F_{|h_{iD}|^2}(x) = \sum_{k=0}^{m_n-1} \Psi(k) \int_0^x t^k e^{-(\beta-\delta)t} dt = \sum_{k=0}^{m_n-1} \frac{\Psi(k)}{(\beta-\delta)^{k+1}} \gamma(k+1, (\beta-\delta)x). \quad (26)$$

Further, using (25) and (26) and denote $\kappa = \frac{\gamma_{out} d_{iD}^{\alpha_S}}{P_i}(\beta-\delta)$, we can be obtain

$$P_{out}^{iD} = \Pr\{\gamma_{iD} \le \gamma_{out}\} = \sum_{k=0}^{m_n-1} \frac{\Psi(k)}{(\beta-\delta)^{k+1}} \gamma\left(k+1, \frac{\gamma_{out} d_{iD}^{\alpha_S}}{P_i}(\beta-\delta) Y\right)$$

$$D_2^{(k)} = \frac{(m_n+k-1)!}{(m_n-1)!} \mathbb{E}_{d_{A_kX}} \left\{ \left(\frac{\Omega}{m_n d_{A_kX}^{\alpha_{R_1}}}\right)^k \left(\frac{d_{A_kX}^{\alpha_{R_1}}}{d_{A_kX}^{\alpha_{R_1}} + \frac{d_{A_mX}^{\alpha_{R_1}} \gamma_{out} P_{A_u}}{P_{A_m}}}\right)^{m_n+k} \right\}$$
$$= \frac{(m_n+k-1)!}{(m_n-1)!} \left(\frac{\Omega}{m_n}\right)^k \int_{d_{\max}^d}^{d_{\max}^u} \frac{x^{\frac{\alpha_{R_1} m_n}{2}}}{\left(x^{\frac{\alpha_{R_1}}{2}} + \Lambda\right)^{m_n+k}} f_{d_{A_kR_1}^2}(x) dx$$
$$= \frac{\pi (m_n+k-1)!}{2V_1 d_{OR_1} (m_n-1)!} \left(\frac{\Omega}{m_n}\right)^k \int_{d_{\max}^d}^{d_{\max}^u} \frac{x^{\frac{\alpha_{R_1} m_n}{2}} [R_A^2 - \tau(x)^2]}{\left(x^{\frac{\alpha_{R_1}}{2}} + \Lambda\right)^{m_n+k}} dx \quad (14)$$

$$D_2^{(k)} = \frac{\pi (m_n+k-1)!}{2V_1 d_{OR_1} (m_n-1)!} \left(\frac{\Omega}{m_n}\right)^k \Lambda^{-m_n-k} \left\{ (R_A^2 - D_{\min}^2) \mathcal{F}\left(\frac{2}{\alpha_{R_1}}, d_{\min}^u, d_{\min}^d, k\right) + (R_A^2 - d_{OR_1}^2) \left[\mathcal{F}\left(\frac{2}{\alpha_{R_1}}, d_{\min}^d, d_{\max}^d, k\right) + \mathcal{F}\left(\frac{2}{\alpha_{R_1}}, d_{\max}^u, d_{\min}^u, k\right) \right] - \left[\mathcal{F}\left(\frac{4}{\alpha_{R_1}}, d_{\min}^d, d_{\max}^d, k\right) + \mathcal{F}\left(\frac{4}{\alpha_{R_1}}, d_{\max}^u, d_{\min}^u, k\right) \right] + 2 d_{OR_1} \left[\mathcal{F}\left(\frac{3}{\alpha_{R_1}}, d_{\min}^d, d_{\max}^d, k\right) + \mathcal{F}\left(\frac{3}{\alpha_{R_1}}, d_{\max}^u, d_{\min}^u, k\right) \right] \right\} \quad (15)$$

$$= \sum_{k=0}^{m_n-1} \frac{\Psi(k)}{(\beta-\delta)^{k+1}} \gamma(k+1, \kappa Y). \quad (27)$$

As shown in [43], $\gamma(k+1,x) < \Gamma(k+1)(1-\exp(-\zeta x))^{k+1}$, $\zeta = (\Gamma(k+2))^{-\frac{1}{k+1}}$. Then, P_{out}^{iD} can be approximated as

$$\begin{aligned} P_{out}^{iD} &\approx \sum_{k=0}^{m_n-1} \frac{\Psi(k)\Gamma(k+1)}{(\beta-\delta)^{k+1}} (1-\exp(-\zeta\kappa Y))^{k+1} \\ &= \sum_{k=0}^{m_n-1} \frac{\Psi(k)\Gamma(k+1)}{(\beta-\delta)^{k+1}} \sum_{t=0}^{k+1} \binom{k+1}{t} (-1)^t \\ &\quad \times \exp(-\zeta\kappa t Y). \end{aligned} \quad (28)$$

Furthermore, considering the randomness of Y, we can obtain

$$\begin{aligned} P_{out}^{iD} &= \sum_{k=0}^{m_n-1} \frac{\Psi(k)\Gamma(k+1)}{(\beta-\delta)^{k+1}} \sum_{t=0}^{k+1} \binom{k+1}{t} \\ &\quad \times (-1)^t \mathbb{E}[\exp(-\zeta\kappa t Y)] \\ &= \sum_{k=0}^{m_n-1} \frac{\Psi(k)\Gamma(k+1)}{(\beta-\delta)^{k+1}} \sum_{t=0}^{k+1} \binom{k+1}{t} \\ &\quad \times (-1)^t \mathscr{L}_Y(\zeta\kappa t), \end{aligned} \quad (29)$$

where $\mathscr{L}_Y(s)$ is the Laplace transform of random variable Y.

Lemma 6: Considering that all jamming channels between the aerial jammers and the terrestrial receiver, D, suffer i.i.d. Nakagmi-m fading, namely, $f_{|h_{jD}|^2}(x) = \left(\frac{m_n}{\Omega}\right)^{m_n} \frac{x^{m_n-1}}{(m_n-1)!} \exp\left(-\frac{m_n}{\Omega}x\right)$, $\mathscr{L}_Y(\zeta\kappa t)$ can be calculated as

$$\begin{aligned} &\mathscr{L}_Y(\zeta\kappa t) \\ &= \exp\left(-\pi R_I \lambda_I \sum_{i=1}^{V} \sqrt{1-t_i^2}\omega_i {\upsilon_i}^2 \right. \\ &\quad \left. \times \left(1 - \left(\frac{m_n}{\Omega}\right)^{m_n} \left(\frac{m_n}{\Omega} + \zeta\kappa t P_j {\upsilon_i}^{-\alpha_S}\right)^{-m_n}\right)\right), \end{aligned} \quad (30)$$

where $\upsilon_i = \frac{R_I(t_i+1)}{2}$, $t_i = \cos\left(\frac{2i-1}{2V}\pi\right)$, and $\omega_i = \frac{\pi}{V}$.

Proof: Please refer to Appendix G.

Therefore, the OP over the downlink can be achieved via inserting (30) into (29).

Adopting the series representations of the exponential function, $\exp\left(-\beta\frac{x}{\lambda_{dn}}\right) = \sum_{n=0}^{\infty} \frac{\left(-\beta\frac{x}{\lambda_{dn}}\right)^n}{n!}$, and keeping the first two terms while ignoring the higher order term, the asymptotic CDF and PDF of $\lambda_{dn} = P_i|h_{iD}|^2$ can be expressed as

$$f_{\lambda_{dn}}^{\infty}(x) = \sum_{k=0}^{m_n-1} \Psi(k) x^k \left(1 - \frac{\beta-\delta}{\lambda_{dn}}x\right) \quad (31)$$

and

$$F_{\lambda_{dn}}^{\infty}(x) = \sum_{k=0}^{m_n-1} \frac{\Psi(k)}{k+1}x^{k+1} - \frac{\Psi(k)(\beta-\delta)}{(k+2)\lambda_{dn}}x^{k+2}. \quad (32)$$

Then, we can obtain P_{out}^{∞} as

$$\begin{aligned} P_{out}^{\infty} = \sum_{k=0}^{m_n-1} &\frac{\Psi(k)}{k+1}(\kappa\mathbb{E}_Y\{Y\})^{k+1} \\ &- \frac{\Psi(k)(\beta-\delta)}{(k+2)\lambda_{dn}}(\kappa\mathbb{E}_Y\{Y\})^{k+2}, \end{aligned} \quad (33)$$

$$\begin{aligned} \mathbb{E}_{d_{A_kX}}\left\{d_{A_kX}^{-\alpha_X}\right\} &= \int_{d_{\max}^d}^{d_{\max}^u} x^{-\frac{\alpha_X}{2}} f_{d_{A_kR_1}^2}(x)dx \\ &= \frac{\pi}{2V_1 d_{OR_1}} \int_{d_{\max}^d}^{d_{\max}^u} x^{-\frac{\alpha_X}{2}} [R_A^2 - \tau(x)^2]dx \\ &= \frac{\pi}{2V_1 d_{OR_1}} \left\{ (R_A^2 - D_{\min}^2) \int_{d_{\min}^d}^{d_{\min}^u} x^{-\frac{\alpha_X}{2}}dx + \int_{d_{\max}^d}^{d_{\min}^d} (R_A^2 - d_{OR_1}^2)x^{-\frac{\alpha_X}{2}} - x^{-\frac{\alpha_X}{2}+1} + 2d_{OR_1}x^{-\frac{\alpha_X-1}{2}})dx \right. \\ &\quad \left. + \int_{d_{\min}^u}^{d_{\max}^u} (R_A^2 - d_{OR_1}^2)x^{-\frac{\alpha_X}{2}} - x^{-\frac{\alpha_X}{2}+1} + 2d_{OR_1}x^{-\frac{\alpha_X-1}{2}})dx \right\} \\ &= \frac{\pi}{2V_1 d_{OR_1}} \left\{ \frac{(R_A^2 - D_{\min}^2)}{-\frac{\alpha_X}{2}+1} \left({d_{\min}^u}^{-\frac{\alpha_X}{2}+1} - {d_{\min}^d}^{-\frac{\alpha_X}{2}+1} \right) + \frac{(R_A^2 - d_{OR_1}^2)}{-\frac{\alpha_X}{2}+1} \left({d_{\min}^d}^{-\frac{\alpha_X}{2}+1} - {d_{\max}^d}^{-\frac{\alpha_X}{2}+1} \right) \right. \\ &\quad - \frac{1}{-\frac{\alpha_X}{2}+2} \left({d_{\min}^d}^{-\frac{\alpha_X}{2}+2} - {d_{\max}^d}^{-\frac{\alpha_X}{2}+2} \right) + \frac{2d_{OR_1}}{-\frac{\alpha_X-1}{2}+1} \left({d_{\min}^d}^{-\frac{\alpha_X-1}{2}+1} - {d_{\max}^d}^{-\frac{\alpha_X-1}{2}+1} \right) \\ &\quad + \frac{(R_A^2 - d_{OR_1}^2)}{-\frac{\alpha_X}{2}+1} \left({d_{\max}^u}^{-\frac{\alpha_X}{2}+1} - {d_{\min}^u}^{-\frac{\alpha_X}{2}+1} \right) - \frac{1}{-\frac{\alpha_X}{2}+2} \left({d_{\max}^u}^{-\frac{\alpha_X}{2}+2} - {d_{\min}^u}^{-\frac{\alpha_X}{2}+2} \right) \\ &\quad \left. + \frac{2d_{OR_1}}{-\frac{\alpha_X-1}{2}+1} \left({d_{\max}^u}^{-\frac{\alpha_X-1}{2}+1} - {d_{\min}^u}^{-\frac{\alpha_X-1}{2}+1} \right) \right\} \end{aligned} \quad (23)$$

where

$$\mathbb{E}_Y\{Y\} = \mathbb{E}_{|h_{jD}|^2, d_{I_j}}\left[\sum_{j=1}^{J}\frac{P_j|h_{jD}|^2}{d_{I_j}^{\alpha_S}}\right] = \sum_{j=1}^{J}\mathbb{E}_{d_{I_j}}\left[\underbrace{\int_0^\infty \frac{P_j|h_{jD}|^2}{d_{I_j}^{\alpha_S}} f_{|h_{jD}|^2}(x)\,dx}_{I_2}\right] = \sum_{j=1}^{J}\left(\lambda_I \int_{\mathbb{R}^3} I_2\left(d_{I_j}\right) dd_{I_j}\right), \tag{34}$$

where

$$I_2 = \left(\frac{m_n}{\Omega}\right)^{m_n}\frac{P_j}{d_{I_j}^{\alpha_S}(m_n-1)!}\int_0^\infty x^{m_n-1}\exp\left(-\frac{m_n}{\Omega}x\right)dx = \left(\frac{m_n}{\Omega}\right)^{-1}\frac{P_j}{d_{I_j}^{\alpha_S}(m_n-1)!}\Gamma(m_n+1), \tag{35}$$

and $\mathbb{R}^3$ is the 3D distribution space for these aerial jammers presented in Fig. 2(b).

Then, $\mathbb{E}_Y\{Y\}$ can be finally derived as

$$\mathbb{E}_Y\{Y\} = \sum_{j=1}^{J}\left(\lambda_I\int_{\mathbb{R}^3} I_2\left(d_{I_j}\right)dd_{I_j}\right) = \sum_{j=1}^{J}\left(-\pi R_I\lambda_I\sum_{i=1}^{V}\sqrt{1-t_i^2}\omega_i {v_i}^2\left(\frac{m_n}{\Omega}\right)^{-1} \times \frac{P_j\Gamma(m_n+1)}{{v_i}^{\alpha_S}(m_n-1)!}\right). \tag{36}$$

Finally, the asymptotic OP over the downlink can be achieved by substituting (36) into (33).

V. Outage of Inter-Aerial Relaying and E2E Links

A. Outage Analysis of Inter-Aerial Relaying Links

Considering Part C of Section II and denoting $\Delta_{n,n+1} = \frac{d_{R_nR_{n+1}}^{\alpha_{R_N}}\sigma^2\gamma_{out}}{P_{R_n}}$, one easily has the OP over the link between the nth ($n=1,\cdots,N-1$) and the $(n+1)$th aerial relays as

$$P_{out}^{R_nR_{n+1}} = \Pr\{\gamma_{R_nR_{n+1}} \le \gamma_{out}\} = \Pr\left\{\frac{P_{R_n}\left|h_{R_nR_{n+1}}\right|^2}{d_{R_nR_{n+1}}^{\alpha_{R_N}}\sigma^2} \le \gamma_{out}\right\} = 1 - \sum_{i=0}^{m_n-1}\left(\frac{m_n}{\Omega}\right)^{m_n-i-1}\frac{\Delta_{n,n+1}^{m_n-i-1}}{(m_n-i-1)!} \times \exp\left(-\frac{m_n}{\Omega}\Delta_{n,n+1}\right). \tag{37}$$

Moreover, here we also assume that the transmission distance over each aerial relay hop is fixed to facilitate the analysis, as the main concern of this work is the impacts of the distribution of the aerial sources and jammers.

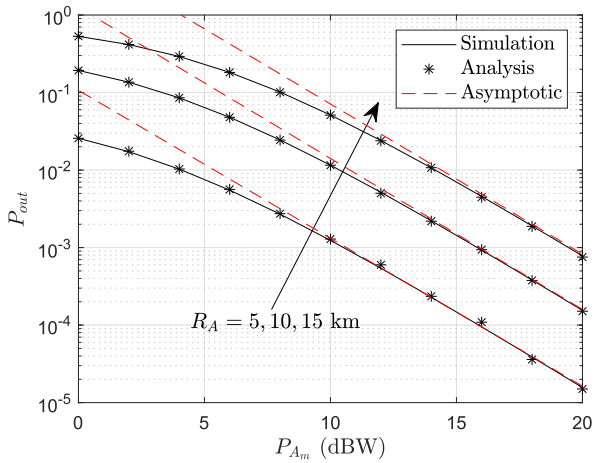

Fig. 3. OP over the uplink for various R_A.

B. E2e OP Analysis

Using the analysis offered in previous sections, the e2e OP of the target system will be presented by considering the adopted relay types.

1) Satellite Relay Link: As observed from Fig. 1 and considering DF scheme is adopted at the satellite, the e2e OP over satellite relay link can be easily written as

$$P_{out}^{SR} = 1 - \left(1 - P_{out}^{OS}\right)\left(1 - P_{out}^{SD}\right). \tag{38}$$

2) Aerial Relay Link: Similar to the previous subsection, we can present the e2e OP over the aerial relay link as

$$P_{out}^{AR} = 1 - \left(1 - P_{out}^{OR_1}\right)\left(1 - P_{out}^{R_ND}\right)\prod_{n=1}^{N-1}\left(1 - P_{out}^{R_nR_{n+1}}\right). \tag{39}$$

VI. Numerical Results

In this section, numerical results will be presented to investigate the performance of the considered cooperative satellite/aerial-terrestrial communication system. We run 10^6 times of the realizations of the considered system and 10^6 trials of Monte-Carlo simulations to model the randomness of the positions of the aerial transmitters and jammers and channel gains over each link.

Following the transmit power and the orbit altitude shown in [44], [45], in this subsection, unless otherwise explicitly specified, the parameters are set as follows: 1) Uplink: $d_{OS} = 300$ km, $R_A = 10$ km, $D_{\min} = 1$ km, $d_{OR_1} = 20$ km, $\alpha_S = 2$, $\alpha_X = 2$, $\gamma_{out} = -1$ dB, $\lambda_A = 1\times10^{-4}$, $m_n = 2$, and $\Omega = 1$; 2) Downlink: $d_{SD} = 300$ km, $R_I = 10$ km, $d_{R_ND} = 20$ km, $\alpha_S = 2$, $\gamma_{out} = -1$ dB, $\lambda_I = 1\times10^{-11}$, $m_n = 2$, $\Omega = 1$, $b = 1$ dB, $P_S = 30$ dBW, and $P_{A_u} = 30$ dBW.

A. The Outage Performance Over the Uplink

Fig. 3 presents the influence of R_A on the outage performance of the uplink. One can see that the OP over the uplink gets worse as the size of the distribution space of the

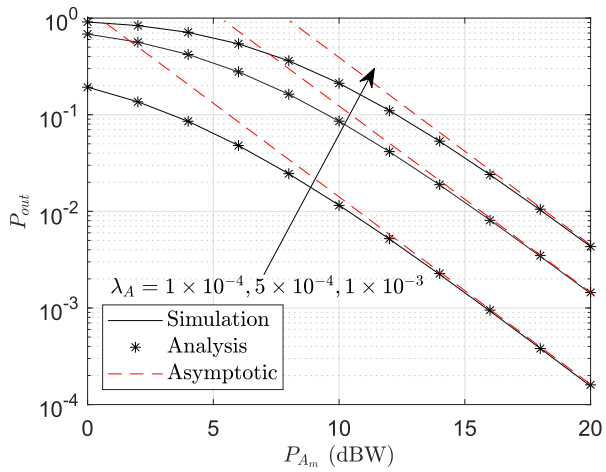

Fig. 4. OP over the uplink for various λ_A.

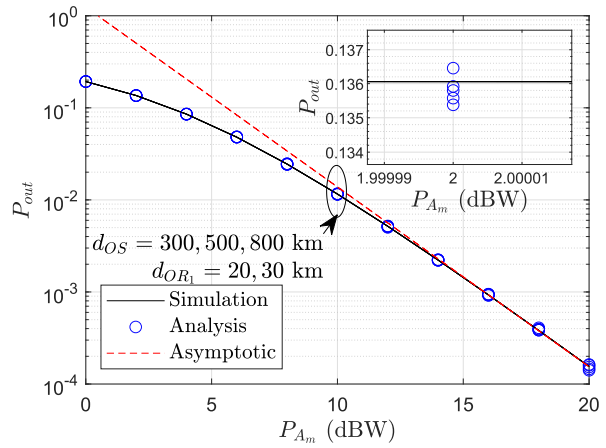

Fig. 5. OP over the uplink for various d_{OS} and d_{OR_1}.

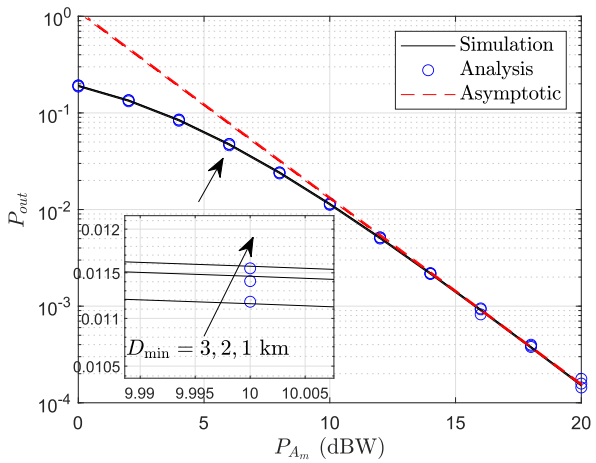

Fig. 6. OP over the uplink for various $D_{\min}$.

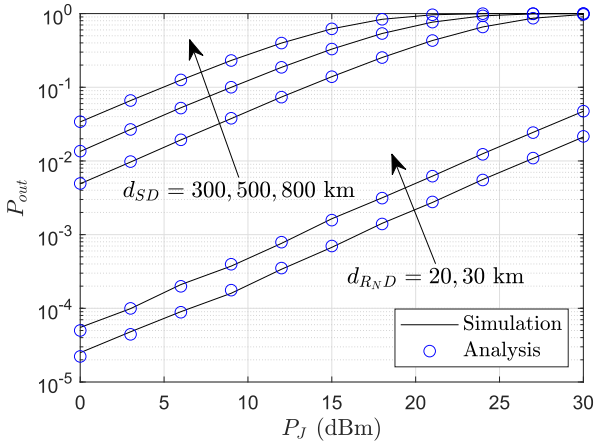

Fig. 7. OP over the downlink for various d_{iD}.

aerial transmitters increases. This observation can be easily understood, since a large distribution space of the aerial transmitters indicates that there will be more aerial transmitters accessing the satellite/the aerial relay simultaneously, resulting in increased MUI accordingly.

Next, in Fig. 4, the impacts of the distribution density of the aerial transmitters on the OP over the uplink are investigated. It is noted from this figure that a large distribution density of the aerial transmitter incurs a reduced outage performance. Because more aerial transmitters will be brought by a large λ_A in the given distribution space, causing large MUI at the satellite/the aerial relay.

Furthermore, the relationship between the OP of the uplink and the transmission distances of the uplink is investigated in Fig. 5. As expected, the transmission distances of the uplink do not have a large impact on the outage performance over the uplink. Because the target transmission signal and corresponding self-interfering signal emitted by other aerial transmitters suffer from the same path loss when traveling over the same uplink.

Finally, the effects of the minimum safety distance among the aerial transmitters, $D_{\min}$, on the outage performance over the uplink are shown in Fig. 6. We can observe that $D_{\min}$ exhibits a positive impact on the OP over the uplink. In other words, a large $D_{\min}$ stands for a small OP over the uplink, which can be interpreted by the fact that for the given distribution space, a large $D_{\min}$ implies a low distribution density of the aerial transmitters and further low MUI at the satellite/the aerial relay. However, one can also see that such a positive effect is very weak as the OP curves plotted in this figure overlap each other from a macroscopic view. Because the range of $D_{\min}$ to promise the safety of the aerial transmitters is relatively quiet smaller than the size of their distribution space and the length of the uplinks.

B. The Outage Performance Over the Downlink

In Figs. 7-9, the OP over the downlink between S/R_N and D is depicted. P_J exhibits an obvious negative impact on the outage performance over the downlink. Because a large P_J represents a large interfering power at D.

In Fig. 7, the OP with different d_{iD} ($i \in \{S, R_N\}$) is presented. The outage performance over the downlink degrades while the transmission distance over the downlink enlarges. More specifically, one can see that the OP over the downlink between the satellite and the terrestrial receiver gets worse when the link length increases from 300 km to 800 km. Similar

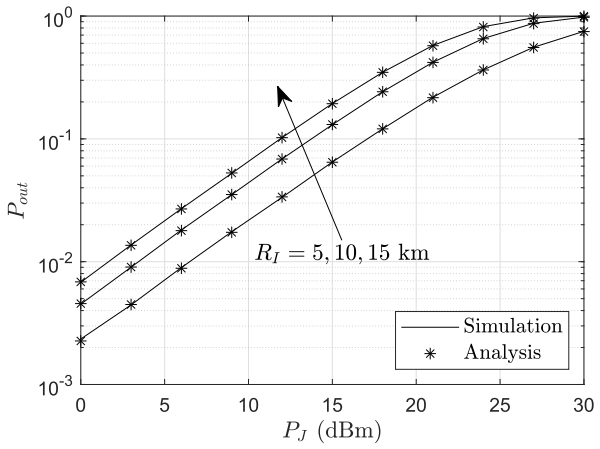

Fig. 8. OP over the downlink for various R_I.

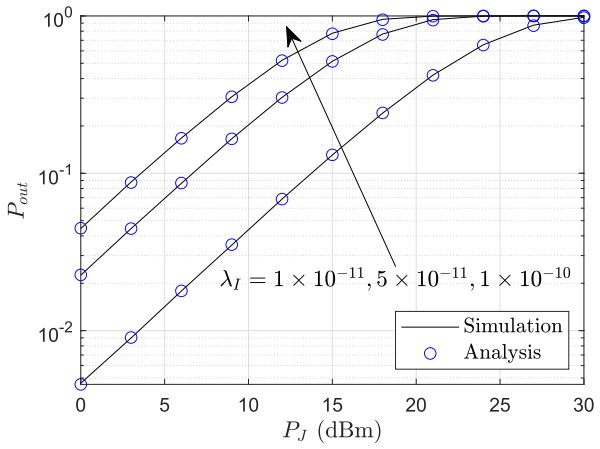

Fig. 9. OP over the downlink for various λ_I.

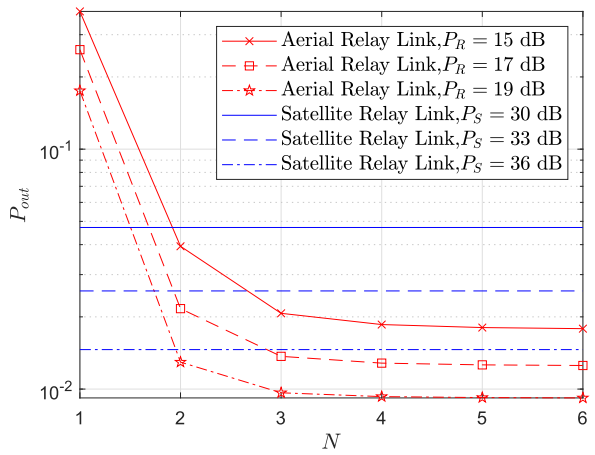

Fig. 10. The e2e OP for various P_S and P_R.

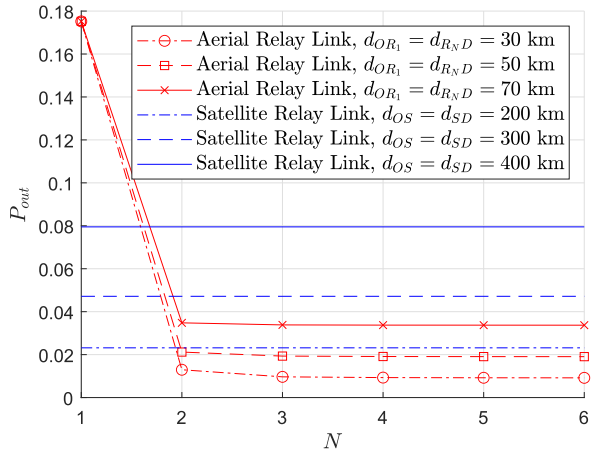

Fig. 11. The e2e OP for various d_{OS}/d_{OR_1} and $d_{SD}/d_{R_N D}$.

observations can be achieved for the downlink between R_N and D when $d_{R_N D}$ reaches 30 km from 20 km.

Fig. 8 studied the influence of the size of the distribution space of the aerial jammers, R_I, on the outage performance over the downlink. The OP over the downlink enlarges while R_I increases. For example, when $P_J = 10$ dBm, the OP of the downlink is on the order of 10^{-3} for $R_I = 5$ km, and that is on the order of 10^{-2} for $R_I = 15$ km. This observation can be easily explained by the fact that a large R_I means a large distribution space and further denotes more aerial jammers, which finally incurs the degraded outage performance.

In Fig. 9, we studied the relationship between the outage performance and the distribution density of the aerial jammers, λ_I. For a given distribution space for the aerial jammers, a large λ_I leads to worse outage performance since a large λ_I implies more aerial jammers operate in the given 3D distribution space. This observation is similar to the one achieved from Fig. 3, which uncovers the impact of the distribution density of the aerial transmitters on the OP over the uplink in the previous subsection.

Moreover, it can be seen from Figs. 3-9 that simulation and analysis results agree with each other very well, which verify the correctness of our proposed analytical models.

C. The E2e Outage Performance

As illustrated in Figs. 10 and 11, for a given transmission distance between the aerial transmitters and the terrestrial destination, N offers a positive impact on the e2e outage performance of the considered system via the aerial relay path, but such a positive influence gets weak while N enlarges as flat bottoms can be seen from the OP lines plotted in both figures. This observation can be explained as follows: The transmission distance between every two neighboring aerial relays gets smaller and smaller when more aerial relays are introduced into the aerial relay link, leading to the improved OP over each aerial relay hop; then, when the outage performance of each aerial relay hop is improved to a certain degree, the e2e outage performance of the considered system will be only decided by the transmission quality over the uplink and the downlink shown in Fig. 2, which agrees with the expression of the e2e OP with aerial relay addressed by (39). Therefore, we can conclude: Though the e2e outage performance can be enhanced somewhat, bringing more aerial relays into the aerial relay link is not always a good choice for the considered system and optimal system design should be carried out to achieve a trade-off between the e2e OP and the increased system resource overhead arisen from the introduced aerial relays.

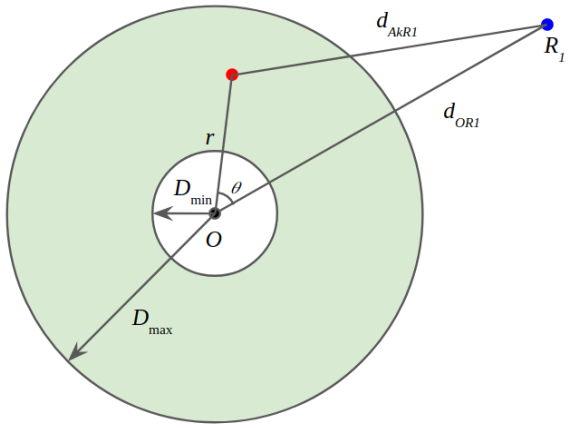

Fig. 12. Aerial transmitter-aerial relay link model.

Moreover, another interesting finding here is that the e2e OP via the satellite relay link does not always outperform that via the aerial relay links because the e2e outage performance under these two cases varies with numerous system factors, e.g., the transmit power at the aerial transmitter/the satellite/the aerial relays, the number of aerial relays, the link distance among all terminals included in the considered system, etc. Thus, to realize an optimal considered system for a practical scenario setting, the selection of the relay link depends on the feasibility of achieving a balance between the e2e OP and other performance indices, for example, the time delay incurred by the multi-hop forwarding over the aerial relay link.

VII. Conclusion

In this work, we have investigated the e2e outage performance of a cooperative SATN, in which there are two relaying choices for a group of aerial sources to forward their information to a remote terrestrial destination. The e2e outage performance of the considered system via two different relay links has been studied and compared. Some remarks are obtained:

1. In presence of co-channel interference among the aerial sources, the transmission distances over the uplinks have a weak impact on the outage performance of the uplinks;
2. The distribution density and the size of the distribution space of the aerial sources and the aerial jammers play a negative role on the OP over the uplink and the downlink, respectively;
3. The safety distance among the aerial sources exhibits a positive impact on the OP over the uplink;
4. For the aerial relay link, the number of aerial relays can be optimized to realize an optimal trade-off between the e2e OP and system resource overhead.
5. The choice of the relay link for the considered system depends on the practical scenario settings. In other words, both two kinds of relay links can provide optimal trade-offs between the e2e outage performance and the other performance indices/constraints, and then people should choose the relay type to satisfy the given system settings.

Appendix A
Proof of Lemma 1

According to the definition of OP, the OP over the link from the mth aerial transmitter to X ($X \in \{S, R_1\}$) can be written as

$$\begin{aligned}
&P_{out}^{A_m X} \\
&= \Pr\{\gamma_{A_m X} \le \gamma_{out}\} \\
&= \Pr\left\{\frac{P_{A_m}|h_{A_m X}|^2 d_{A_m X}^{-\alpha_X}}{\sum\limits_{k=1\&k\neq m}^{M} P_{A_k}|h_{A_k X}|^2 d_{A_k X}^{-\alpha_X}} \le \gamma_{out}\right\} \\
&= \Pr\left\{|h_{A_m X}|^2 \le \frac{d_{A_m X}^{\alpha_X}\gamma_{out}P_{A_u}}{P_{A_m}} \sum_{k=1\&k\neq m}^{M} |h_{A_k X}|^2 d_{A_k X}^{-\alpha_X}\right\} \\
&= 1 - \sum_{i=0}^{m_n-1} \frac{(-1)^{m_i}}{(m_i)!}\mathbb{E}_{I,d_{A_m X}}\left\{(sI)^{m_i}\exp(sI)\right\} \\
&= 1 - \sum_{i=0}^{m_n-1} \frac{(-1)^{m_i}}{(m_i)!}\mathbb{E}_{d_{A_m X}}\left\{s^{m_i}\underbrace{\mathbb{E}_I\left\{I^{m_i}\exp(sI)\right\}}_{D_1}\right\},
\end{aligned} \tag{40}$$

where $I = \sum\limits_{k=1\&k\neq m}^{M} |h_{A_k X}|^2 d_{A_k X}^{-\alpha_X}$ and $s = -\frac{m_n d_{A_m X}^{\alpha_X}\gamma_{out}P_{A_u}}{P_{A_m}\Omega}$.

It is easy to get

$$D_1 = \frac{\mathrm{d}^{m_i}\mathbb{E}_I\left\{\exp(sI)\right\}}{\mathrm{d}s^{m_i}}. \tag{41}$$

Thus, we can obtain (8) via substituting (41) into (40).

Appendix B
Proof of Lemma 2

As $|h_{A_k X}|^2$ and $d_{A_k X}$ are i.i.d random variables, we can get

$$\begin{aligned}
&\mathbb{E}_I\left\{\exp(sI)\right\} \\
&= \mathbb{E}_M\left\{\mathbb{E}_{|h_{A_k X}|^2, d_{A_k X}}\left\{\exp\left(s\sum_{k=1\&k\neq m}^{M}\frac{|h_{A_k X}|^2}{d_{A_k X}^{\alpha_X}}\right)\right\}\right\} \\
&= \mathbb{E}_M\left\{\prod_{k=1\&k\neq m}^{M}\mathbb{E}_{|h_{A_k X}|^2, d_{A_k X}}\left\{\exp\left(\frac{s|h_{A_k X}|^2}{d_{A_k X}^{\alpha_X}}\right)\right\}\right\} \\
&= \sum_{M=0}^{\infty}\frac{(\lambda_A V_1)^M}{M!}\exp(-\lambda_A V_1) \\
&\quad\times\left\{\underbrace{\mathbb{E}_{|h_{A_k X}|^2, d_{A_k X}}\left\{\exp\left(\frac{s|h_{A_k X}|^2}{d_{A_k X}^{\alpha_X}}\right)\right\}}_{D_2}\right\}^M \\
&= \sum_{M=0}^{\infty}\frac{(\lambda_A V_1 D_2)^M}{M!}\exp(-\lambda_A V_1) \\
&= \exp\left[\lambda_A V_1(D_2 - 1)\right],
\end{aligned} \tag{42}$$

where $V_1 = \frac{4\pi}{3}(R_A^3 - D_{\min}^3)$.

Using the moment generating function (MGF) of $|h_{A_kX}|^2$, it deduces

$$D_2 = \mathbb{E}_{d_{A_kX}}\left\{\left(\frac{\frac{m_n}{\Omega s}d_{A_kX}^{\alpha_X}}{\frac{m_n}{\Omega s}d_{A_kX}^{\alpha_X}-1}\right)^{m_n}\right\}. \tag{43}$$

Then, (9) can be reached by combining (42) and (43).

Appendix C
Proof of Lemma 3

After achieving $\mathbb{E}_I\{\exp(sI)\}$, we will derive its (m_i)th derivative. We know that the 0th derivative of any function is itself. When $m_i > 0$, according to the Faàdi Bruno's formula, we can get

$$\begin{aligned}&\frac{\mathrm{d}^{m_i}\mathbb{E}_I\{\exp(sI)\}}{\mathrm{d}s^{m_i}}\\ &= \exp[\lambda_A V_1(D_2-1)]\sum_{k=1}^{m_i}B_{m_i,k}\\ &\quad\times\left(\lambda_A V_1 D_2^{(1)},\ldots,\lambda_A V_1 D_2^{(m_i-k+1)}\right),\end{aligned} \tag{44}$$

where $B_{m,k}(\cdot)$ is the Bell polynomials and $D_2^{(k)}$ is the kth derivative of D_2 w.r.t. s.

It is easy to get $D_2^{(k)}$ after substituting $s = -\frac{m_n d_{A_mX}^{\alpha_X}\gamma_{out}P_{A_u}}{P_{A_m}\Omega}$ as

$$\begin{aligned}D_2^{(k)} &= \frac{(m_n+k-1)!}{(m_n-1)!}\mathbb{E}_{d_{A_kX}}\left\{\left(\frac{\Omega}{m_n d_{A_kX}^{\alpha_X}}\right)^k\right.\\ &\quad\left.\times\left(\frac{m_n d_{A_kX}^{\alpha_X}}{m_n d_{A_kX}^{\alpha_X}-\Omega s}\right)^{m_n+k}\right\}\\ &= \frac{(m_n+k-1)!}{(m_n-1)!}\mathbb{E}_{d_{A_kX}}\left\{\left(\frac{\Omega}{m_n d_{A_kX}^{\alpha_X}}\right)^k\right.\\ &\quad\left.\times\left(\frac{d_{A_kX}^{\alpha_X}}{d_{A_kX}^{\alpha_X}+\frac{d_{A_mX}^{\alpha_X}\gamma_{out}P_{A_u}}{P_{A_m}}}\right)^{m_n+k}\right\}.\end{aligned} \tag{45}$$

Substituting (44), (45), and $s = -\frac{m_n d_{A_mX}^{\alpha_X}\gamma_{out}P_{A_u}}{P_{A_m}\Omega}$ into (8), the OP can be presented as (10).

Appendix D
Proof of Lemma 4

As aerial transmitters are assumed to be independently and uniformly distributed in $\mathcal{V}$, the joint CDF of r and θ can be expressed as

$$\begin{aligned}F_{r,\theta}(x,y) &= \frac{\int_0^{2\pi}d\varphi\int_0^{y}\sin\theta d\theta\int_{D_{\min}}^{x}r^2dr}{V_1}\\ &= \frac{2\pi(1-\cos y)(x^3-D_{\min}^3)}{3V_1}.\end{aligned} \tag{46}$$

Then, the joint PDF of r and θ can be written as

$$f_{r,\theta}(x,y) = \frac{\partial^2 F_{r,\theta}(x,y)}{\partial x\partial y} = \frac{2\pi x^2\sin y}{V_1}. \tag{47}$$

From Fig. 12, the relationships between r, θ, and $d_{A_kR_1}^2$ can be represented as $d_{A_kR_1}^2 = r^2 + d_{OR_1}^2 - 2rd_{OR_1}\cos\theta$. It can be easily seen that $d_{OR_1} - R_A \le d_{A_kR_1} \le d_{OR_1} + R_A$. To obtain the PDF of $d_{A_kR_1}^2$, we first derive the joint PDF of $d_{A_kR_1}^2$ and r.

According to the multivariate change of variables formula, the Jacobian determinant of matrix $\partial(d_{A_kR_1}^2, r)/\partial(r,\theta)$ is

$$\begin{aligned}\left|\frac{\partial(d_{A_kR_1}^2,r)}{\partial(r,\theta)}\right| &= \begin{vmatrix}2r-2d_{OR_1}\cos\theta & 2rd_{OR_1}\sin\theta\\ 1 & 0\end{vmatrix}\\ &= 2rd_{OR_1}\sin\theta.\end{aligned} \tag{48}$$

Then, the joint PDF of $d_{A_kR_1}^2$ and r can be achieved as

$$f_{d_{A_kR_1}^2,r}(x,y) = \frac{f_{r,\theta}(x,y)}{\left|\frac{\partial(d_{A_kR_1}^2,r)}{\partial(r,\theta)}\right|} = \frac{\pi y}{V_1 d_{OR_1}}, \tag{49}$$

where $D_{\min} \le y \le R_A$ and $-1 \le \cos\theta = \frac{y^2+d_{OR_1}^2-x}{2d_{OR_1}y} \le 1$.

From $-1 \le \cos\theta = \frac{y^2+d_{OR_1}^2-x}{2d_{OR_1}y} \le 1$, we can get $x \le (d_{OR_1}+y)^2$ and $(d_{OR_1}-y)^2 \le x$. As $R_A \ll d_{OR_1}$, one can obtain $\sqrt{x} - d_{OR_1} \le y$ and $d_{OR_1} - \sqrt{x} \le y$, namely, $|\sqrt{x} - d_{OR_1}| \le y$. Observing $D_{\min} \le y \le R_A$, the range of y is $\max\{D_{\min}, |\sqrt{x}-d_{OR_1}|\} \le y \le R_A$.

The PDF of $d_{A_kR_1}^2$ can be acquired through the integration of $f_{d_{A_kR_1}^2,r}(x,y)$ in (49) according to r and finally shown in (13).

Appendix E
Proof of (15)

By using [42, Eq. (3.194.1)], $D_2^{(k)}$ can be obtained as (50), shown at the bottom of the next page, where $\mathcal{F}(a,b,c,k) = \Big[b^{\frac{(m_n+a)\alpha_{R_1}}{2}}{}_2F_1 m_n+k, m_n+am_n+a+1-\frac{b^{\frac{\alpha_{R_1}}{2}}}{\Lambda} - c^{\frac{(m_n+a)\alpha_{R_1}}{2}}{}_2F_1 m_n+k, m_n+am_n+a+1-\frac{c^{\frac{\alpha_{R_1}}{2}}}{\Lambda}\Big]\times\frac{2}{(m_n+a)\alpha_{R_1}}$.

Appendix F
Proof of Lemma 5

By substituting (17) into (40), we can obtain that

$$\begin{aligned}P_{out}^{\infty} &= 1-\sum_{i=0}^{m_n-1}\frac{(-1)^{m_i}}{(m_i)!}\mathbb{E}_{I,d_{A_mX}}\{(sI)^{m_i}(1-sI)\}\\ &= 1-\sum_{i=0}^{m_n-1}\frac{(-1)^{m_i}}{(m_i)!}\mathbb{E}_{d_{A_mX}}\{s^{m_i}\mathbb{E}_I\{I^{m_i}(1-sI)\}\}\\ &= 1-\sum_{i=0}^{m_n-1}\frac{(-1)^{m_i}}{(m_i)!}\{\mathbb{E}_{d_{A_mX}}\{s^{m_i}\}\mathbb{E}_I\{I^{m_i}\}\\ &\quad-\mathbb{E}_{d_{A_mX}}\{s^{m_i+1}\}\mathbb{E}_I\{I^{m_i+1}\}\}.\end{aligned} \tag{51}$$

As $|h_{A_kX}|^2$ and d_{A_kX} are i.i.d random variables, $\mathbb{E}_I\{I\}$ can be derived as

$$\mathbb{E}_I\{I\} = \mathbb{E}_M\left\{\mathbb{E}_{|h_{A_kX}|^2,d_{A_kX}}\left\{\sum_{k=1\&k\neq m}^{M}\frac{|h_{A_kX}|^2}{d_{A_kX}^{\alpha_X}}\right\}\right\}$$

$$
\begin{aligned}
&= \sum_{M=0}^{\infty} \frac{(\lambda_A V_1)^M}{(M-1)!} \exp\left(-\lambda_A V_1\right) \\
&\quad \times \mathbb{E}_{|h_{A_k X}|^2}\left\{|h_{A_k X}|^2\right\} \mathbb{E}_{d_{A_k X}}\left\{d_{A_k X}^{-\alpha_X}\right\} \\
&= \sum_{M=0}^{\infty} \frac{(\lambda_A V_1)^M}{(M-1)!} \exp\left(-\lambda_A V_1\right) \\
&\quad \times \left\{1 - \sum_{i=0}^{m_n-1} \left(\frac{m_n}{\Omega}\right)^{m_n-i-1} \frac{x^{m_n-i}}{(m_n-i-1)!} \right. \\
&\quad \left. \times \exp\left(-\frac{m_n}{\Omega} x\right)\right\} \mathbb{E}_{d_{A_k X}}\left\{d_{A_k X}^{-\alpha_X}\right\}. \qquad (52)
\end{aligned}
$$

Then, (18) can be reached by combining (51) and (52).

APPENDIX G: PROOF OF LEMMA 6

As it has been assumed that the channels between the aerial jammers and the terrestrial receiver, D, suffer i.i.d. Nakagmi-m fading, we have $f_{|h_{jD}|^2}(x) = \left(\frac{m_n}{\Omega}\right)^{m_n} \frac{x^{m_n-1}}{(m_n-1)!} \exp\left(-\frac{m_n}{\Omega} x\right)$. Thus, we derive $\mathscr{L}[Y](s)$ as

$$
\begin{aligned}
\mathscr{L}_Y(s) &= \mathbb{E}\left[\exp\left(-sY\right)\right] = \mathbb{E}\left[\exp\left(-s\sum_{j=1}^{J} \frac{P_j |h_{jD}|^2}{d_{I_j}^{\alpha_S}}\right)\right] \\
&= \mathbb{E}\left[\prod_{j=1}^{J} \exp\left(-\frac{s P_j |h_{jD}|^2}{d_{I_j}^{\alpha_S}}\right)\right] \\
&= \mathbb{E}\left[\prod_{j=1}^{J} \underbrace{\int_0^{\infty} \exp\left(-\frac{s P_j |h_{jD}|^2}{d_{I_j}^{\alpha_S}}\right) f_{|h_{jD}|^2}(x)\, dx}_{I_1}\right] \\
&= \exp\left(-\lambda_I \int_{\mathbb{R}^3} \left(1 - I_1\left(d_I\right)\right) d d_I\right), \qquad (53)
\end{aligned}
$$

$$
\begin{aligned}
D_2^{(k)} &= \frac{\pi(m_n+k-1)!}{2V_1 d_{OR_1}(m_n-1)!} \left(\frac{\Omega}{m_n}\right)^k \left\{(R_A^2 - D_{\min}^2) \int_{d_{\min}^d}^{d_{\min}^u} \frac{x^{\frac{\alpha_{R_1} m_n}{2}}}{\left(x^{\frac{\alpha_{R_1}}{2}} + \Lambda\right)^{m_n+k}} dx \right. \\
&\quad + \int_{d_{\max}^d}^{d_{\min}^d} \frac{(R_A^2 - d_{OR_1}^2) x^{\frac{\alpha_{R_1} m_n}{2}} - x^{\frac{\alpha_{R_1} m_n}{2}+1} + 2 d_{OR_1} x^{\frac{\alpha_{R_1} m_n+1}{2}})}{\left(x^{\frac{\alpha_{R_1}}{2}} + \Lambda\right)^{m_n+k}} dx \\
&\quad \left. + \int_{d_{\min}^u}^{d_{\max}^u} \frac{(R_A^2 - d_{OR_1}^2) x^{\frac{\alpha_{R_1} m_n}{2}} - x^{\frac{\alpha_{R_1} m_n}{2}+1} + 2 d_{OR_1} x^{\frac{\alpha_{R_1} m_n+1}{2}})}{\left(x^{\frac{\alpha_{R_1}}{2}} + \Lambda\right)^{m_n+k}} dx \right\} \\
&= \frac{\pi(m_n+k-1)!}{2V_1 d_{OR_1}(m_n-1)!} \left(\frac{\Omega}{m_n}\right)^k \Lambda^{-m_n-k} \frac{2}{\alpha_{R_1}} \left\{(R_A^2 - D_{\min}^2) \int_{d_{\min}^d}^{d_{\min}^u} \frac{x^{\frac{\alpha_{R_1}}{2}\left(m_n-1+\frac{2}{\alpha_{R_1}}\right)}}{\left(\frac{x^{\frac{\alpha_{R_1}}{2}}}{\Lambda} + 1\right)^{m_n+k}} dx^{\frac{\alpha_{R_1}}{2}} \right. \\
&\quad + \int_{d_{\max}^d}^{d_{\min}^d} \frac{(R_A^2 - d_{OR_1}^2) x^{\frac{\alpha_{R_1}}{2}\left(m_n-1+\frac{2}{\alpha_{R_1}}\right)} - x^{\frac{\alpha_{R_1}}{2}\left(m_n-1+\frac{4}{\alpha_{R_1}}\right)} + 2 d_{OR_1} x^{\frac{\alpha_{R_1}}{2}\left(m_n-1+\frac{3}{\alpha_{R_1}}\right)}}{\left(\frac{x^{\frac{\alpha_{R_1}}{2}}}{\Lambda} + 1\right)^{m_n+k}} dx^{\frac{\alpha_{R_1}}{2}} \\
&\quad \left. + \int_{d_{\min}^u}^{d_{\max}^u} \frac{(R_A^2 - d_{OR_1}^2) x^{\frac{\alpha_{R_1}}{2}\left(m_n-1+\frac{2}{\alpha_{R_1}}\right)} - x^{\frac{\alpha_{R_1}}{2}\left(m_n-1+\frac{4}{\alpha_{R_1}}\right)} + 2 d_{OR_1} x^{\frac{\alpha_{R_1}}{2}\left(m_n-1+\frac{3}{\alpha_{R_1}}\right)}}{\left(\frac{x^{\frac{\alpha_{R_1}}{2}}}{\Lambda} + 1\right)^{m_n+k}} dx^{\frac{\alpha_{R_1}}{2}} \right\} \\
&= \frac{\pi(m_n+k-1)!}{2V_1 d_{OR_1}(m_n-1)!} \left(\frac{\Omega}{m_n}\right)^k \Lambda^{-m_n-k} \left\{(R_A^2 - D_{\min}^2) \mathcal{F}\left(\frac{2}{\alpha_{R_1}}, d_{\min}^u, d_{\min}^d, k\right) \right. \\
&\quad + (R_A^2 - d_{OR_1}^2) \left[\mathcal{F}\left(\frac{2}{\alpha_{R_1}}, d_{\min}^d, d_{\max}^d, k\right) + \mathcal{F}\left(\frac{2}{\alpha_{R_1}}, d_{\max}^u, d_{\min}^u, k\right)\right] \\
&\quad - \left[\mathcal{F}\left(\frac{4}{\alpha_{R_1}}, d_{\min}^d, d_{\max}^d, k\right) + \mathcal{F}\left(\frac{4}{\alpha_{R_1}}, d_{\max}^u, d_{\min}^u, k\right)\right] \\
&\quad \left. + 2 d_{OR_1} \left[\mathcal{F}\left(\frac{3}{\alpha_{R_1}}, d_{\min}^d, d_{\max}^d, k\right) + \mathcal{F}\left(\frac{3}{\alpha_{R_1}}, d_{\max}^u, d_{\min}^u, k\right)\right] \right\} \qquad (50)
\end{aligned}
$$

$$\begin{aligned}\mathscr{L}_Y(s) &= \exp\left(-\lambda_I \int_0^{R_I}\int_0^{\frac{\pi}{2}}\int_0^{2\pi}\left(1-\left(\frac{m_n}{\Omega}\right)^{m_n}\left(\frac{m_n}{\Omega}+\frac{sP_j}{r^{\alpha_S}}\right)^{-m_n}\right) r^2\sin\phi d\psi d\phi dr\right)\\ &= \exp\left(-2\pi\lambda_I \int_0^{R_I} r^2\left(1-\left(\frac{m_n}{\Omega}\right)^{m_n}\left(\frac{m_n}{\Omega}+\frac{sP_j}{r^{\alpha_S}}\right)^{-m_n}\right) dr \int_0^{\frac{\pi}{2}}\sin\phi d\phi\right)\\ &= \exp\left(-2\pi\lambda_I \int_0^{R_I} r^2\left(1-\left(\frac{m_n}{\Omega}\right)^{m_n}\left(\frac{m_n}{\Omega}+\frac{sP_j}{r^{\alpha_S}}\right)^{-m_n}\right) dr\right)\\ &= \exp\left(-\pi R_I\lambda_I \sum_{i=1}^{V}\sqrt{1-t_i^2}\omega_i {\upsilon_i}^2\left(1-\left(\frac{m_n}{\Omega}\right)^{m_n}\left(\frac{m_n}{\Omega}+\frac{sP_j}{{\upsilon_i}^{\alpha_S}}\right)^{-m_n}\right)\right) \end{aligned} \tag{55}$$

where $\mathbb{R}^3$ is the 3D distribution space for these aerial jammers presented in Fig. 2(b),

$$\begin{aligned} I_1 &= \left(\frac{m_n}{\Omega}\right)^{m_n}\frac{1}{(m_n-1)!}\int_0^{\infty} x^{m_n-1}\\ &\quad\times\exp\left(-\left(\frac{m_n}{\Omega}+\frac{sP_j}{d_{I_j}^{\alpha_S}}\right)x\right)dx\\ &= \left(\frac{m_n}{\Omega}\right)^{m_n}\left(\frac{m_n}{\Omega}+\frac{sP_j}{d_{I_j}^{\alpha_S}}\right)^{-m_n}, \end{aligned} \tag{54}$$

and the last step follows the probability generating functional of the PPP, which means for function $f(x)$ that $\mathbb{E}\left[\prod_{\mathbb{R}} f(x)\right] = \exp\left(-\lambda\int_0^{\infty}\left(1-f(x)\right)dx\right)$.

Then, thinking that $\mathbb{R}^3$ is a hemisphere space depicted in Fig. 2(b), one can finally derive $\mathscr{L}_Y(s)$ as (55), shown at the top of the page, where $\upsilon_i = \frac{R_I(t_i+1)}{2}$, $t_i = \cos\left(\frac{2i-1}{2V}\pi\right)$, and $\omega_i = \frac{\pi}{V}$.

Finally, replacing s in (55) by $\zeta\kappa t$ accomplishes the proof of Lemma 5.

REFERENCES

[1] J. Liu, Y. Shi, Z. M. Fadlullah, and N. Kato, "Space-air-ground integrated network: A survey," *IEEE Commun. Surveys Tuts.*, vol. 20, no. 4, pp. 2714–2741, 4th Quart., 2018.

[2] Y. Ruan, Y. Li, C.-X. Wang, and R. Zhang, "Energy efficient adaptive transmissions in integrated satellite-terrestrial networks with SER constraints," *IEEE Trans. Wireless Commun.*, vol. 17, no. 1, pp. 210–222, Jan. 2018.

[3] R. Deng, B. Di, H. Zhang, L. Kuang, and L. Song, "Ultra-dense LEO satellite constellations: How many LEO satellites do we need?" *IEEE Trans. Wireless Commun.*, vol. 20, no. 8, pp. 4843–4857, Aug. 2021.

[4] G. Pan, J. Ye, Y. Zhang, and M.-S. Alouini, "Performance analysis and optimization of cooperative satellite-aerial-terrestrial systems," *IEEE Trans. Wireless Commun.*, vol. 19, no. 10, pp. 6693–6707, Oct. 2020.

[5] Q. Huang, M. Lin, J. Wang, T. A. Tsiftsis, and J. Wang, "Energy efficient beamforming schemes for satellite-aerial-terrestrial networks," *IEEE Trans. Commun.*, vol. 68, no. 6, pp. 3863–3875, Jun. 2020.

[6] J. Li, K. Xue, D. S. L. Wei, J. Liu, and Y. Zhang, "Energy efficiency and traffic offloading optimization in integrated satellite/terrestrial radio access networks," *IEEE Trans. Wireless Commun.*, vol. 19, no. 4, pp. 2367–2381, Apr. 2020.

[7] Y. Wang, W. Feng, J. Wang, and T. Q. S. Quek, "Hybrid satellite-UAV-terrestrial networks for 6G ubiquitous coverage: A maritime communications perspective," *IEEE J. Sel. Areas Commun.*, vol. 39, no. 11, pp. 3475–3490, Nov. 2021.

[8] L. Yin and B. Clerckx, "Rate-splitting multiple access for multigroup multicast and multibeam satellite systems," *IEEE Trans. Commun.*, vol. 69, no. 2, pp. 976–990, Feb. 2021.

[9] B. Wu, F. Fang, and S. Fu, "Improving the system performance in terrestrial-satellite relay networks by configuring aerial relay," *IEEE Trans. Veh. Technol.*, vol. 70, no. 12, pp. 13139–13148, Dec. 2021.

[10] X. Li, W. Feng, Y. Chen, C.-X. Wang, and N. Ge, "Maritime coverage enhancement using UAVs coordinated with hybrid satellite-terrestrial networks," *IEEE Trans. Commun.*, vol. 68, no. 4, pp. 2355–2369, Apr. 2020.

[11] F. Pervez, L. Zhao, and C. Yang, "Joint user association, power optimization and trajectory control in an integrated satellite-aerial-terrestrial network," *IEEE Trans. Wireless Commun.*, vol. 21, no. 5, pp. 3279–3290, May 2022.

[12] Q. Wang, H. Zhang, J.-B. Wang, F. Yang, and G. Y. Li, "Joint beamforming for integrated mmWave satellite-terrestrial self-backhauled networks," *IEEE Trans. Veh. Technol.*, vol. 70, no. 9, pp. 9103–9117, Sep. 2021.

[13] Z. Gao, A. Liu, C. Han, and X. Liang, "Max completion time optimization for Internet of Things in LEO satellite-terrestrial integrated networks," *IEEE Internet Things J.*, vol. 8, no. 12, pp. 9981–9994, Jun. 2021.

[14] L. Wang, Y. Wu, H. Zhang, S. Choi, and V. C. M. Leung, "Resource allocation for NOMA based space-terrestrial satellite networks," *IEEE Trans. Wireless Commun.*, vol. 20, no. 2, pp. 1065–1075, Feb. 2021.

[15] P. Deyi, A. Bandi, Y. Li, S. Chatzinotas, and B. Ottersten, "Hybrid beamforming, user scheduling, and resource allocation for integrated terrestrial-satellite communication," *IEEE Trans. Veh. Technol.*, vol. 70, no. 9, pp. 8868–8882, Sep. 2021.

[16] X. Zhu, C. Jiang, L. Kuang, and Z. Zhao, "Cooperative multilayer edge caching in integrated satellite-terrestrial networks," *IEEE Trans. Wireless Commun.*, vol. 21, no. 5, pp. 2924–2937, May 2022.

[17] Y. Ruan, Y. Li, C.-X. Wang, R. Zhang, and H. Zhang, "Energy efficient power allocation for delay constrained cognitive satellite terrestrial networks under interference constraints," *IEEE Trans. Wireless Commun.*, vol. 18, no. 10, pp. 4957–4969, Oct. 2019.

[18] Y. Tian, G. Pan, M. A. Kishk, and M.-S. Alouini, "Stochastic analysis of cooperative satellite-UAV communications," *IEEE Trans. Wireless Commun.*, vol. 21, no. 6, pp. 3570–3586, Jun. 2022.

[19] J. Ye, G. Pan, and M.-S. Alouini, "Earth rotation-aware non-stationary satellite communication systems: Modeling and analysis," *IEEE Trans. Wireless Commun.*, vol. 20, no. 9, pp. 5942–5956, Sep. 2021.

[20] G. Pan, J. Ye, Y. Tian, and M.-S. Alouini, "On HARQ schemes in satellite-terrestrial transmissions," *IEEE Trans. Wireless Commun.*, vol. 19, no. 12, pp. 7998–8010, Dec. 2020.

[21] G. Pan, J. Ye, J. An, and S. Alouini, "Latency versus reliability in LEO mega-constellations: Terrestrial, aerial, or space relay," *IEEE Trans. Mobile Comput.*, early access, Apr. 19, 2022, doi: 10.1109/TMC.2022.3168081.

[22] C. Li, H. Zhu, J. Cai, J. Hu, G. Li, and G. Li, "Capacity analysis of terrestrial antenna array in distributed satellite MIMO communication system," *IEEE Trans. Veh. Technol.*, vol. 70, no. 5, pp. 4435–4450, May 2021.

[23] X. Yue *et al.*, "Outage behaviors of NOMA-based satellite network over Shadowed–Rician fading channels," *IEEE Trans. Veh. Technol.*, vol. 69, no. 6, pp. 6818–6821, Jun. 2020.
[24] P. K. Sharma, D. Gupta, and D. I. Kim, "Outage performance of 3D mobile UAV caching for hybrid satellite-terrestrial networks," *IEEE Trans. Veh. Technol.*, vol. 70, no. 8, pp. 8280–8285, Aug. 2021.
[25] N. Okati, T. Riihonen, D. Korpi, I. Angervuori, and R. Wichman, "Downlink coverage and rate analysis of low Earth orbit satellite constellations using stochastic geometry," *IEEE Trans. Commun.*, vol. 68, no. 8, pp. 5120–5134, Aug. 2020.
[26] Y. Zhang, J. Ye, G. Pan, and M.-S. Alouini, "Secrecy outage analysis for satellite-terrestrial downlink transmissions," *IEEE Wireless Commun. Lett.*, vol. 9, no. 10, pp. 1643–1647, Oct. 2020.
[27] S. A. Tegos, P. D. Diamantoulakis, J. Xia, L. Fan, and G. K. Karagiannidis, "Outage performance of uplink NOMA in land mobile satellite communications," *IEEE Wireless Commun. Lett.*, vol. 9, no. 10, pp. 1710–1714, Oct. 2020.
[28] H. Lin, C. Zhang, Y. Huang, R. Zhao, and L. Yang, "Fine-grained analysis on downlink LEO satellite-terrestrial mmWave relay networks," *IEEE Wireless Commun. Lett.*, vol. 10, no. 9, pp. 1871–1875, Sep. 2021.
[29] Z. Zhao, G. Xu, N. Zhang, and Q. Zhang, "Symbol error analysis of amplify-and-forward based multiuser hybrid satellite-terrestrial relay network," *IEEE Wireless Commun. Lett.*, vol. 10, no. 10, pp. 2279–2283, Oct. 2021.
[30] X. Liang, J. Jiao, S. Wu, and Q. Zhang, "Outage analysis of multirelay multiuser hybrid satellite-terrestrial millimeter-wave networks," *IEEE Wireless Commun. Lett.*, vol. 7, no. 6, pp. 1046–1049, Dec. 2018.
[31] A. Agarwal and P. Kumar, "Analysis of variable bit rate SOFDM transmission scheme over multi-relay hybrid satellite-terrestrial system in the presence of CFO and phase noise," *IEEE Trans. Veh. Technol.*, vol. 68, no. 5, pp. 4586–4601, May 2019.
[32] W. Zeng, J. Zhang, D. W. K. Ng, B. Ai, and Z. Zhong, "Two-way hybrid terrestrial-satellite relaying systems: Performance analysis and relay selection," *IEEE Trans. Veh. Technol.*, vol. 68, no. 7, pp. 7011–7023, Jul. 2019.
[33] L. Han, W.-P. Zhu, and M. Lin, "Outage analysis of NOMA-based multiple-antenna hybrid satellite-terrestrial relay networks," *IEEE Commun. Lett.*, vol. 25, no. 4, pp. 1109–1113, Apr. 2021.
[34] X. Zhang, B. Zhang, K. An, G. Zheng, S. Chatzinotas, and D. Guo, "Stochastic geometry-based analysis of cache-enabled hybrid satellite-aerial-terrestrial networks with non-orthogonal multiple access," *IEEE Trans. Wireless Commun.*, vol. 21, no. 2, pp. 1272–1287, Feb. 2022.
[35] X. Liu, C. Gu, K. Guo, M. Cheng, M. Lin, and W.-P. Zhu, "Robust beamforming and outage performance of uplink multiuser satellite-aerial-terrestrial networks with mixed RF-FSO channels," *IEEE Photon. J.*, vol. 13, no. 4, pp. 1–8, Aug. 2021.
[36] J. Ye, S. Dang, B. Shihada, and M.-S. Alouini, "Space-air-ground integrated networks: Outage performance analysis," *IEEE Trans. Wireless Commun.*, vol. 19, no. 12, pp. 7897–7912, Dec. 2020.
[37] K. Guo and K. An, "On the performance of RIS-assisted integrated satellite-UAV-terrestrial networks with hardware impairments and interference," *IEEE Wireless Commun. Lett.*, vol. 11, no. 1, pp. 131–135, Jan. 2022.
[38] P. K. Sharma and D. I. Kim, "Secure 3D mobile UAV relaying for hybrid satellite-terrestrial networks," *IEEE Trans. Wireless Commun.*, vol. 19, no. 4, pp. 2770–2784, Apr. 2020.
[39] P. K. Singya and M.-S. Alouini, "Performance of UAV-assisted multiuser terrestrial-satellite communication system over mixed FSO/RF channels," *IEEE Trans. Aerosp. Electron. Syst.*, vol. 58, no. 2, pp. 781–796, Apr. 2022.
[40] *Propagation Data and Prediction Methods Required for the Design of Earth-Space Telecommunication Systems*, document ITU-R Recommendation P.618-12, Feb. 2007. Accessed: May 30, 2022. [Online]. Available: https://www.itu.int/dms_pubrec/itu-r/rec/p/R-REC-P.682-2-200702-S!!PDF-E.pdf
[41] A. Abdi, W. C. Lau, M.-S. Alouini, and M. Kaveh, "A new simple model for land mobile satellite channels: First- and second-order statistics," *IEEE Trans. Wireless Commun.*, vol. 2, no. 3, pp. 519–528, May 2003.
[42] I. S. Gradshteyn and I. M. Ryzhik, *Table of Integrals, Series and Products*, 7th ed. San Diego, CA, USA: Academic, 2007.
[43] H. Alzer, "On some inequalities for the incomplete gamma function," *Math. Comput.*, vol. 66, pp. 771–778, Apr. 1997.
[44] N. H. Crisp *et al.*, "System modelling of very low Earth orbit satellites for Earth observation," *Acta Astronautica*, vol. 187, pp. 475–491, Oct. 2021.
[45] *Technical Characteristics for Telemetry, Tracking and Command in the Space Operation Service Below 1 GHz for Non-GSO Satellites With Short Duration Missions*, document ITU-R SA.2426-0, Sep. 2018. Accessed: May 30, 2022. [Online]. Available: https://www.itu.int/pub/R-REP-SA.2426

Zhe Song received the bachelor's and master's degrees from the School of Information and Electronics, Beijing Institute of Technology, in 2009 and 2012, respectively, where she is currently pursuing the Ph.D. degree with the Institute of Aerospace Information Networks. Her research interests include the physical and link layer issues of satellite communications and space information networks.

Jianping An (Senior Member, IEEE) received the Ph.D. degree from the Beijing Institute of Technology, China, in 1996. He joined the School of Information and Electronics, Beijing Institute of Technology, in 1995, where he is currently a Full Professor. He is also currently the Dean of the School of Information and Electronics, Beijing Institute of Technology. His research interests include digital signal processing, wireless communications, and satellite networks. He has received two national awards for technological inventions and science and technology progress.

Gaofeng Pan (Senior Member, IEEE) received the B.Sc. degree in communication engineering from Zhengzhou University, Zhengzhou, China, in 2005, and the Ph.D. degree in communication and information systems from Southwest Jiaotong University, Chengdu, China, in 2011. He is currently with the School of Cyberspace Science and Technology, Beijing Institute of Technology, China, as a Professor. His research interests span special topics in communications theory, signal processing, and protocol design.

Shuai Wang (Senior Member, IEEE) received the Ph.D. degree in communications systems from the Beijing Institute of Technology (BIT), China, in 2012. Upon his graduation, he joined the Faculty of the School of Information and Electronics, BIT. In 2021, he transferred to the new-founded School of Cyberspace Science and Technology where he was appointed as the Chair Professor with the Department for Information Security and Countermeasures. He has contributed over 40 peer-reviewed articles, mainly in leading IEEE journals or conferences and holds over 60 patents. His research interests include satellite communications, anti-interference communications, and datalink technologies for space platforms. He was the co-recipient of the 2nd Class National Technical Invention Award of China in 2019. He served as the Editor for IEEE WIRELESS COMMUNICATIONS LETTERS and is serving as the Editor for *China Communications*.

Haoxing Zhang (Student Member, IEEE) received the B.Sc. degree in communication engineering from the Beijing Institute of Technology, China, in 2018, where she is currently pursuing the Ph.D. degree with the School of Cyberspace Science and Technology. Her main research interests include the performance analysis and modeling of wireless communication systems.

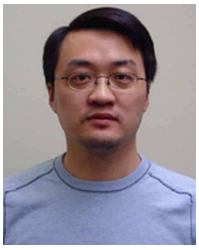

Yunfei Chen (Senior Member, IEEE) received the B.E. and M.E. degrees in electronics engineering from Shanghai Jiao Tong University, Shanghai, China, in 1998 and 2001, respectively, and the Ph.D. degree from the University of Alberta in 2006. He is currently working as an Associate Professor with The University of Warwick, U.K. His research interests include wireless communications, cognitive radios, wireless relaying, and energy harvesting.

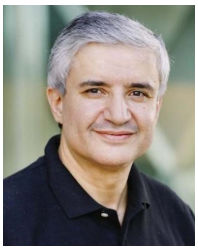

Mohamed-Slim Alouini (Fellow, IEEE) was born in Tunis, Tunisia. He received the Ph.D. degree in electrical engineering from the California Institute of Technology (Caltech), Pasadena, CA, USA, in 1998. He served as a Faculty Member with the University of Minnesota, Minneapolis, MN, USA, then with the Texas A&M University at Qatar, Education City, Doha, Qatar, before joining the King Abdullah University of Science and Technology (KAUST), Thuwal, Makkah, Saudi Arabia, as a Professor of electrical engineering in 2009. His current research interests include modeling, design, and performance analysis of wireless communication systems.